Article

# Dual neuromodulatory dynamics underlie birdsong learning

https://doi.org/10.1038/s41586-025-08694-9

Received: 8 November 2023

Accepted: 23 January 2025

Published online: 12 March 2025

Check for updates

Jiaxuan Qi[1], Drew C. Schreiner[1], Miles Martinez[1,2], John Pearson[1,2,3] ✉ & Richard Mooney[1] ✉

Although learning in response to extrinsic reinforcement is theorized to be driven by dopamine signals that encode the difference between expected and experienced rewards[1,2], skills that enable verbal or musical expression can be learned without extrinsic reinforcement. Instead, spontaneous execution of these skills is thought to be intrinsically reinforcing[3,4]. Whether dopamine signals similarly guide learning of these intrinsically reinforced behaviours is unknown. In juvenile zebra finches learning from an adult tutor, dopamine signalling in a song-specialized basal ganglia region is required for successful song copying, a spontaneous, intrinsically reinforced process[5]. Here we show that dopamine dynamics in the song basal ganglia faithfully track the learned quality of juvenile song performance on a rendition-by-rendition basis. Furthermore, dopamine release in the basal ganglia is driven not only by inputs from midbrain dopamine neurons classically associated with reinforcement learning but also by song premotor inputs, which act by means of local cholinergic signalling to elevate dopamine during singing. Although both cholinergic and dopaminergic signalling are necessary for juvenile song learning, only dopamine tracks the learned quality of song performance. Therefore, dopamine dynamics in the basal ganglia encode performance quality during self-directed, long-term learning of natural behaviours.

Learning occurs when behaviour changes in response to reinforcement[6]. Theories of reinforcement learning posit that this process is driven by a discrepancy between expected and experienced rewards—the reward prediction error (RPE)—long identified with dopamine (DA) release in the basal ganglia (BG)[1,2]. Yet although many impressive forms of motor learning, including the imitative learning that gives rise to speech or musical expression in humans, are also thought to rely on this mechanism, they do not depend on extrinsic reward or punishment; instead, the spontaneous execution of these skills is believed to be intrinsically reinforcing[3,4]. One hint that DA may convey an RPE-like signal in these types of learning is that DA dynamics in the BG of the mouse correlate with and can reinforce spontaneously executed movements[7], although how this process is organized into self-directed and long-term learning of natural, adaptive behaviours is unknown.

A juvenile male zebra finch 'pupil' memorizes and then vocally imitates the multisyllabic song motif of an adult male 'tutor' in a process of sensorimotor learning with many parallels to speech and music learning[8–10] (Fig. 1a). Sensorimotor learning involves extensive vocal practice, during which the juvenile sings tens to hundreds of thousands of song renditions over many weeks and evaluates the quality of these renditions using auditory feedback[11–13]. Remarkably, sensorimotor learning proceeds without any reinforcement other than this practice[14,15], indicating that singing is intrinsically reinforcing.

A primary locus of sensorimotor learning is a song-specialized region of the BG (sBG) that is active during singing but not other behaviours and that is a primary target of dopaminergic signalling[5,16–18] (Fig. 1b). During juvenile sensorimotor learning, DA signals that encode performance quality are speculated to modify pallial–sBG circuitry to trigger rapid changes in song that are consolidated more slowly in downstream song motor circuits[19,20] (Fig. 1b). Notably, in adult finches, DA neurons in the midbrain ventral tegmental area (VTA) that innervate the sBG encode an RPE-like signal in response to natural fluctuations in syllable quality[21] and to syllable-triggered noise[22]. Furthermore, performance-contingent optogenetic manipulation of VTA terminals in the sBG can be used to alter the fundamental frequency (pitch) of a target syllable[5,23]. However, unlike adult pitch learning, sensorimotor learning in juveniles involves simultaneous changes across many acoustic dimensions for each syllable, and syllables are executed in a rapid sequence, all without external reinforcement. Moreover, in other organisms, local DA release is affected by factors other than the activity of VTA cell bodies[24–26], raising the question of whether DA dynamics in the sBG encode an RPE-like signal during juvenile learning.

Here we used fibre photometry to longitudinally image singing-related DA transients in the juvenile's sBG using genetically encoded DA sensors[27], a method that encompasses both DA release resulting from the action potential activity of DA cell bodies and axonal release mechanisms local to the BG. We then used computational methods to retrospectively quantify the maturity of individual syllable renditions relative to the final learned song[12,13], finding that DA dynamics in the sBG faithfully track rendition-to-rendition fluctuations in the maturity of individual syllables. Surprisingly, we also found that DA transients can be evoked in the sBG not only by the VTA but also by song

[1]Department of Neurobiology, Duke University School of Medicine, Durham, NC, USA. [2]Department of Electrical and Computer Engineering, Duke University, Durham, NC, USA. [3]Department of Biostatistics and Bioinformatics, Duke University, Durham, NC, USA. ✉e-mail: john.pearson@duke.edu; mooney@neuro.duke.edu

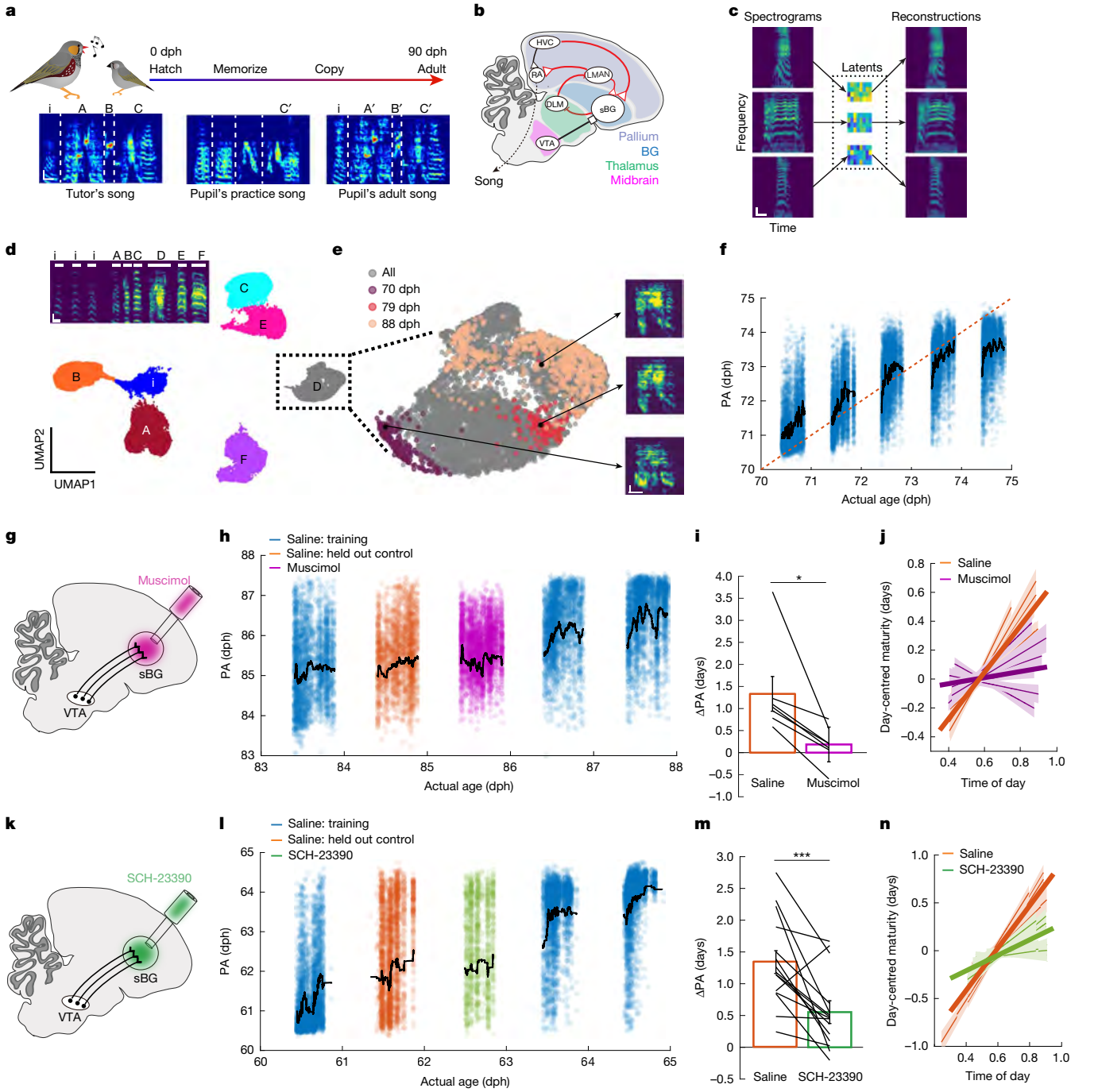


**Fig. 1 | Syllable maturation requires neural activity and DA signalling in the sBG. a**, Song learning timeline (top); spectrograms of tutor's song and pupil's song during and after learning (bottom). i, introductory note; A–C, syllables comprising the motif. **b**, Sagittal view of the song system, emphasizing pallial song premotor (HVC, high vocal centre; LMAN, lateral part of the magnocellular nucleus of the nidopallium) and motor (RA, robust nucleus of the arcopallium) nuclei; the sBG; DLM (dorsolateral part of the medial thalamus) and VTA. **c**, VAEs compressively encode syllable spectrograms into latent embeddings. **d**, UMAP projections of latent embeddings of syllable renditions (A–F) recorded across sensorimotor learning. **e**, All renditions of syllable 'D' (grey dots) and renditions from days 70 (purple), 79 (red) and 88 (tan), with example spectrograms at right. **f**, VAE–ANNs' predicted syllable age versus the actual age of production (dots, individual renditions; black line, rolling average). **g**, Muscimol microdialysis to reversibly inactivate the sBG. **h**, Predicted versus actual age for syllable renditions on saline days used to train the ANN (blue), saline control day (orange) and muscimol day (purple). Black, rolling average. **i**, sBG inactivation reduces daily syllable maturation (PA change from first to last 50 renditions, saline versus muscimol, $n = 7$ syllables, five juveniles, $t_6 = 3.412$, $P = 0.0143$, two-tailed paired $t$-test). **j**, sBG inactivation significantly reduced increases in day-centred PA (linear mixed-effects model; interaction between treatment (saline or muscimol) and time of day, $t_{40102} = -16.498$, $P = 6.0334 \times 10^{-61}$, two-tailed $t$-test). **k**, SCH-23390 microdialysis to reversibly block D1Rs in the sBG. **l**, Predicted versus actual age on ANN training control days (blue), saline control (orange) and SCH-23390 treatment (green) days. **m**,**n**, Blocking D1Rs in the sBG reduces daily syllable maturation assessed either by means of PA change (**m**) ($n = 15$ syllables, seven juveniles, $t_{14} = 4.182$, $P = 0.0009$, two-tailed paired $t$-test) or by the slope of day-centred maturity (**n**) (linear mixed-effects model, interaction between treatment (saline or SCH-23390) and time of day, $t_{70280} = 18.936$, $P = 9.0833 \times 10^{-80}$, two-tailed $t$-test). **i**,**m**, Boxes and error bars, mean ± s.e.m. **j**,**n**, Dark lines, mean slope per group; lighter lines, posterior estimates for individual syllables; shaded regions, 95% confidence intervals. $^{*}P < 0.05$, $^{**}P < 0.01$, $^{***}P < 0.001$. Scale bars, 1 kHz (vertical), 50 ms (horizontal). dph, days post hatch. Panel **a** adapted from ref. 10, Cell Press.

premotor inputs to the sBG, the latter of which act by means of cholinergic signalling mechanisms to elevate DA in the sBG during singing. These results establish that DA dynamics in the sBG convey an RPE-like signal during sensorimotor learning in juvenile finches.

## DA signals in the sBG are needed for song learning

Following memorization of a tutor song, a juvenile male zebra finch sings many thousands of song renditions each day for more than a month, ultimately 'crystallizing' an adult song that closely resembles the memorized tutor model (Fig. 1a). Every song rendition comprises a motif of 2–7 syllables, each of which is acoustically complex and variable from one rendition to the next. We used a recently developed three-step computational method[13] to rigorously characterize this complex sensorimotor learning process in a cohort of previously tutored juvenile male zebra finches. After recording a large corpus of a juvenile's songs during a period that spanned much of sensorimotor learning, individual song motifs were segmented into their component syllables. For each juvenile, sound spectrograms of these segmented syllables were used to train a variational autoencoder (VAE), which compressed the high-dimensional image (128 × 128, or about 16,000 pixels) into a low- (32-) dimensional latent embedding through its encoder arm and accurately reconstructed this spectrogram through its decoder arm[12] (Fig. 1c). For visualization purposes, these 32-dimensional latent embeddings of the syllable renditions produced during sensorimotor learning can be projected onto two dimensions using uniform manifold approximation and projection (UMAP) and colour-coded for the age of production (Fig. 1d,e). Qualitatively, this method of visualizing syllable development showed changes in most (30 of 34) syllable distributions over sensorimotor learning (Fig. 1e and Extended Data Fig. 1a; 34 syllables from ten juvenile males; see Extended Data Table 1 for a summary of birds used in this study).

To quantify this developmental progression in syllable acoustics, we trained an artificial neural network (ANN) to infer the age at which a syllable rendition was most likely to have been produced (predicted age (PA), which we also refer to as 'maturity') from its latent acoustic representation. As previously reported[13], this VAE–ANN method showed that PA values for individual renditions in any single day could vary widely but that the mean PA increased about 1 day each day (Fig. 1f and Extended Data Fig. 1b; $n = 34$ syllables from ten juvenile males). To explore how the sBG contributes to these daily changes in syllable maturity, we used microdialysis methods in another group of juvenile males to infuse drugs into the sBG on a single day, restricting ANN training to a narrower developmental window that bracketed this drug treatment day. Reversibly dialysing the sBG with muscimol, a $GABA_A$ receptor agonist that suppresses action potential activity in neuronal cell bodies, almost completely abolished the daily increase in syllable maturity (Fig. 1g–j and Extended Data Fig. 1c; $n = 7$ syllables from five juvenile males). A similar approach showed that blocking D1-type DA receptors in the sBG strongly attenuated daily increases in syllable maturity (Fig. 1k–n; $n = 15$ syllables from seven juvenile males). A linear mixed-effects model showed a significant interaction between drug treatment and time of day for both treatment groups, indicating that learning was impaired across the drug treatment day (Fig. 1j,n). Furthermore, the effects of blocking neuronal activity or D1 receptors (D1Rs) in the sBG on PA scores were still significant when they were normalized to the total amount of singing (Extended Data Fig. 1d–g). Finally, neither of these drug treatments altered various acoustic features of individual syllables, as measured using either the VAE–ANN or a custom sound analysis program, Sound Analysis Pro 2011 (SAP; http://soundanalysispro.com/) (Extended Data Fig. 1h–q). Therefore, neuronal activity and D1R-mediated DA signalling in the sBG are necessary for daily changes in syllable maturity that characterize sensorimotor learning.

## DA dynamics encode syllable maturity

Having established the importance of DA signalling in the sBG to sensorimotor learning, we explored the relationship between DA dynamics in the sBG and rendition-to-rendition variations in syllable maturity. We used viral vectors to express a genetically encoded DA sensor, GRAB-DA2m[27], in the sBG of adult male zebra finches and confirmed with fibre photometry that electrical stimulation in the VTA (a primary source of DA terminals in the sBG[17]) elicited transient increases in fluorescence in the sBG (Fig. 2a–c and Extended Data Fig. 2a,b; $n = 8$ adult males). Fibre photometric recordings detected robust singing-related DA transients in the sBG of adult male zebra finches that tracked the onset, duration and offset of song bouts (a rapid string of motifs); such transients were not detected in GFP-expressing birds (Fig. 2d–f and Extended Data Fig. 2c–f; $n = 12$ GRAB-DA adult males, $n = 4$ GFP adult males). We then expressed GRAB-DA2m in the sBG of five juvenile male zebra finches and recorded songs and singing-related DA transients in the sBG during sensorimotor learning. We also confirmed in these juvenile birds that the DA transients in the sBG were specific to singing and not other non-vocal movements (Extended Data Fig. 2g,h). At the end of the final imaging session, we trained a VAE–ANN on recordings of each juvenile's song and generated maturity scores for every rendition of every segmentable syllable in the bird's song ($n = 21$ syllables from five juvenile males). To better characterize the relative changes in maturity during each imaging session, we also calculated the session-centred maturity (that is, PA scores mean-centred in each 5-min imaging session). We further established that the session-centred maturity of each syllable was not correlated with that of other syllables in the motif or between the same or different syllables across different motifs (Extended Data Fig. 2i–l), indicating that maturity varies independently at the level of individual syllables. Consequently, we focused on a syllable-level analysis that related the magnitude of DA transients in the sBG to the learned quality of syllable performance, as captured by the syllable's maturity.

Using a combination of cross-correlation methods and predictive modelling, we found that relative changes in a syllable's maturity between renditions were most predictive of the DA signal 100–300 ms after syllable onset (Fig. 2g,h), even when accounting for other acoustic variables (Extended Data Fig. 2m). Guided by these analyses, we used two independent approaches to test the hypothesis that DA transients in the sBG are correlated with changes in syllable maturity. First, we calculated the rendition-to-rendition change in PA scores for each syllable (ΔPA), allowing us to inspect changes in syllable maturity that were notably more progressive or regressive than the previous rendition of that syllable (Extended Data Fig. 2n,o). Analysis of the GRAB-DA2m signals associated with these ΔPA scores showed that DA transients in the sBG were significantly higher on renditions that showed the largest increases in PA relative to the previous rendition (Fig. 2i–l and Extended Data Fig. 2p–r; $n = 21$ syllables from five juvenile males). However, models of reinforcement learning posit that DA transients should track performance quality in a more continuous manner, not only at the upper and lower margins of performance. Therefore, we analysed the relationship between the magnitude of DA transients in the sBG and continuous changes in syllable maturity as quantified by session-centred maturity. This more continuous analysis showed a positive relationship between the magnitude of the DA transient in the sBG and the relative maturity scores for all syllables (Fig. 2m–o). Along with our finding that DA signalling in the sBG is necessary for daily increases in syllable maturity (Fig. 1k–n), these findings indicate that singing-related DA dynamics in the sBG quantitatively reflect changes in song performance.

One possible explanation is that DA dynamics reflect simple functions of performance, rather than more complex features related to learning. However, no acoustic feature had a consistent relationship with either ΔPA or session-centred maturity, indicating that PA is not

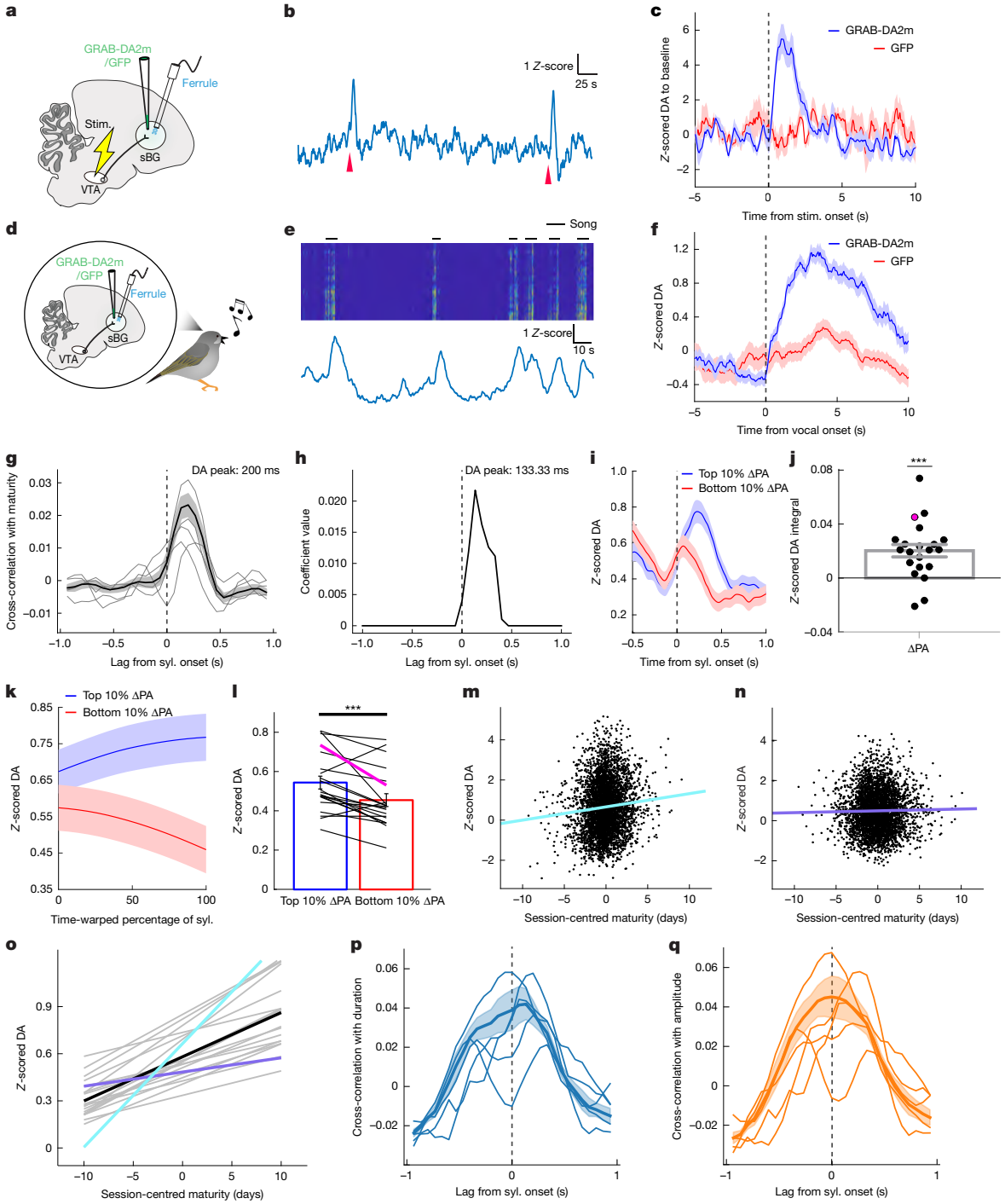


**Fig. 2 | DA dynamics in the sBG encode syllable maturity. a**,**b**, Measuring DA in the sBG evoked by VTA stimulation (stim.) (**a**) (arrowheads (**b**)). **c**, Mean isosbestic-corrected *Z*-scored fluorescence signal evoked by VTA stimulation in a GRAB-DA adult bird (blue, $n = 6$ trials; replicated in 8 of 8 GRAB-DA adults) and in a GFP adult bird (red, $n = 7$ trials, replicated in 3 of 3 GFP adults). **d**, Measuring singing-evoked DA in the sBG. **e**, Representative DA transients during several song bouts. **f**, Singing-related fluorescence in the sBG aligned to song onset recorded with GRAB-DA2m (blue, 67 songs, one adult bird; replicated in 12 of 12 adults) or GFP (red, 77 songs, one adult bird; replicated in 4 of 4 adults). **g**, Cross-correlation between session-centred maturity and DA peaks about 200 ms after syllable (syl.) onset ($n = 5$ juveniles). **h**, LASSO-regularized coefficients peak 133 ms after syllable onset ($n = 5$ juveniles). **i**, Mean DA transients for top (blue) and bottom (red) deciles of ΔPA renditions (443 per decile) of an example syllable. **j**, Areal difference between top and bottom mean ΔPA scores (0.1–0.3 s after syllable onset; 21 syllables, five juveniles; $t_{20} = 4.404$, $P = 0.0003$, one-sample two-tailed *t*-test). Magenta dot is syllable in **i**. **k**, Time-warped DA transients with 100-ms lag for top and bottom decile ΔPA syllable renditions in **i**. **l**, Mean time-warped DA transients for top and bottom decile ΔPA renditions (21 syllables, five birds; $t_{20} = 3.955$, $P = 0.0008$, two-tailed paired *t*-test). Magenta line is syllable in **k**. **m**,**n**, Posterior estimated slopes from the linear mixed-effects model in the syllable with the strongest (**m**; slope = 0.0659, $R^2 = 9.89 \times 10^{-5}$) and weakest (**n**; slope = 0.0090, $R^2 = 4.13 \times 10^{-6}$) relationship between session-centred maturity and DA. Each point is a syllable rendition. **o**, Linear mixed-effects model showing a significant correlation between DA transients and session-centred maturity (21 syllables, five birds, $\beta = 0.02813$, $t_{11.546} = 5.125$, $P = 2.84 \times 10^{-4}$, two-tailed *t*-test). Cyan and purple lines from **m** and **n**; dark line, mean; grey lines, posterior means for each syllable. **p**,**q**, Cross-correlation between DA and syllable duration (**p**) or amplitude (**q**). **c**,**f**,**i**,**k**, Dark line and shaded region, mean and s.e.m. **g**,**p**,**q**, Thin lines, individual birds; dark line and shaded region, group mean and s.e.m. **j**,**l**, Boxes and error bars denote mean ± s.e.m. $^{*}P < 0.05$, $^{**}P < 0.01$, $^{***}P < 0.001$.

simply a proxy for specific acoustic features (Extended Data Fig. 2s,t). Another possibility is that in addition to encoding information important to learning, DA signals also encode movement vigour, as reported in the mammalian BG[28,29]. Therefore, we also analysed the relationship between DA dynamics in the sBG and various acoustic features of song syllables, some of which may reflect song vigour. This analysis showed that the magnitude of the singing-related DA transient in the sBG positively correlated with syllable duration, amplitude and pitch goodness but not with a wide variety of other features (Extended Data Fig. 2u). Syllable amplitude and duration were not correlated, indicating they are independent features (Extended Data Fig. 2v). However, neither duration, amplitude nor pitch goodness correlated with changes in syllable maturity (ΔPA) (Extended Data Fig. 2w). These observations indicate that DA transients in the sBG independently encode information about syllable maturity and vigour. In support of this idea, cross-correlation analyses showed that DA signals associated with duration and amplitude increased before syllable onset (Fig. 2p,q), in contrast to the DA signal associated with maturity, which began to rise only after syllable onset (Fig. 2g). In summary, the most parsimonious explanation is that DA levels in the sBG correlate with syllable maturity and independently with acoustic features that may reflect aspects of song vigour.

## Canonical and non-canonical DA release in the sBG

A notable feature of the DA signal we recorded in the sBG is that it always increased from baseline levels during singing, regardless of song quality. This contrasts with the action potential firing rates of the VTA DA neurons that innervate the sBG, which are not elevated above baseline firing rates during normal singing[30]. This discrepancy raises the possibility that DA release in the sBG is regulated by circuit mechanisms that operate independently of action potentials in VTA DA cell bodies[24–26]. In fact, in the course of conducting what we initially regarded as a control experiment for VTA stimulation (Fig. 2a–c and Extended Data Fig. 2b), we observed that electrical stimulation in the ipsilateral HVC, a pallial song premotor input to the sBG[31], routinely evoked DA transients in the sBG (Fig. 3a,b and Extended Data Fig. 3a; $n = 8$ adult males). This is surprising because the HVC neurons that innervate the sBG are glutamatergic (VGLUT2$^+$) and do not express tyrosine hydroxylase, the enzyme required for DA synthesis (Extended Data Fig. 3b,c). Moreover, electrical stimulation in the contralateral HVC failed to evoke DA transients in the sBG, indicating that the DA transient evoked by ipsilateral HVC stimulation was not simply a non-specific effect of electrical stimulation of the brain (Extended Data Fig. 3d, $n = 4$ adult males).

In the rodent striatum, release of acetylcholine (ACh) from cholinergic interneurons (CINs) can activate nicotinic receptors on DA terminals, triggering DA release[24–26]. Furthermore, CINs can be excited by glutamatergic input from the cortex[32,33], providing a pathway by which cortical activity can potentially modulate DA release in the striatum. We used several approaches to explore whether a similar circuit mechanism contributed to the singing-related increase in DA in the sBG. First, we virally expressed a genetically engineered ACh sensor, GRAB-ACh3.0 (ref. 34), in the sBG of adult male zebra finches (Extended Data Fig. 3e). Similar to the DA transients evoked in the sBG by electrical stimulation of the ipsilateral HVC, electrical stimulation in the ipsilateral but not contralateral HVC triggered ACh transients in the sBG (Fig. 3c,d, $n = 7$ adult males; Extended Data Fig. 3f, $n = 7$ adult males). Notably, the ACh transient evoked by the ipsilateral HVC stimulation was strongly reduced by the systemic injection of scopolamine, a selective antagonist of the type 3 muscarinic receptor from which GRAB-ACh3.0 was derived[34] (Extended Data Fig. 3g,h, $n = 5$ adult males). Furthermore, in contrast to stimulation-evoked DA transients, stimulation in the ipsilateral VTA failed to evoke ACh transients in the sBG (Extended Data Fig. 3f, $n = 5$ adult males). We then used an anterograde intersectional method to selectively label neurons in the sBG receiving synaptic inputs from HVC axons[35]. Injection of AAV2/1-hsyn-Cre in HVC and AAV2/1 or AAV2/9-CAG-FLEX-GFP in the ipsilateral sBG resulted in GFP expression in choline acetyltransferase (ChAT$^+$) neurons in the sBG, as well as in DARPP32$^+$ neurons and other cells (Fig. 3e–i and Extended Data Fig. 3i; $n = 83$ GFP$^+$ neurons in 12 hemispheres from six adult males). Furthermore, infusing the nAChR α4β2 subunit antagonist DHβE into the sBG reduced DA transients evoked by HVC stimulation, but not those evoked by VTA stimulation (Fig. 3j–n; $n = 6$ adult males for HVC stimulation, $n = 5$ adult males for VTA stimulation). Finally, we confirmed that the tyrosine hydroxylase + VTA cells that project to the sBG express mRNA that encodes the α4 subunit of nAChRs (CHRNA4, Extended Data Fig. 3j). Collectively, these data indicate that HVC axon terminals can drive DA release in the sBG through a local mechanism involving ChAT$^+$ neurons and nAChRs located on DA terminals arising from VTA cell bodies.

The HVC neurons that project to the sBG exhibit robust increases in action potential activity during singing[36] and thus could act through this local cholinergic mechanism to help drive singing-related increases in DA in the sBG. Consistent with this idea, fibre photometric recordings detected robust singing-related ACh transients in the sBG of adult male zebra finches that tracked the onset, duration and offset of song bouts, similar to the singing-related action potential activity of putative CINs recorded in the sBG of male zebra finches[37] and similar to singing-related DA transients in the sBG recorded here (Fig. 3o–q and Extended Data Figs. 2c–f and 3k–n; $n = 6$ adult males). Local inhibition of nAChRs by infusing DHβE through an optofluidic cannula strongly reduced singing-related DA transients in the sBG without reducing song duration, a variable that could influence the magnitude of the GRAB-DA signal (Fig. 3r–v, Extended Data Table 2 and Extended Data Fig. 2e; $n = 6$ adult males). Therefore, singing-related DA transients in the sBG depend in part on a process where an HVC-dependent elevation of ACh activates nAChRs in the sBG to trigger DA release.

## DA and ACh contribute differently to song learning

The current finding that a cholinergic mechanism regulates DA release in the sBG during singing raises the possibility that ACh has an important role in sensorimotor learning. Consistent with this possibility, we found that reversibly dialysing the sBG with DHβE strongly reduced daily syllable maturation (Fig. 4a–c and Extended Data Fig. 4a; $n = 11$ syllables from 4 juvenile males). A linear mixed-effects model also showed a significant interaction between DHβE treatment and time of day (Fig. 4d). Furthermore, DHβE's effect on PA scores was still significant when normalized to the total amount of singing (Extended Data Fig. 4b,c). Notably, SAP and VAE–ANN analysis of various syllable acoustic features (Extended Data Fig. 4e–h) showed that DHβE increased the mean of the frequency modulation (Extended Data Fig. 4e) and reduced pitch variability (Extended Data Fig. 4g). Although either of these effects could possibly impair vocal exploration necessary to sensorimotor learning, DHβE's effects on mean frequency modulation and pitch variability did not correlate with the effects of DHβE on daily changes in syllable maturity (Extended Data Fig. 4i,j). Therefore, DHβE treatment may affect syllable maturation through other mechanisms, perhaps by reducing singing-evoked DA tone in the sBG (Fig. 3r–v).

A remaining issue is whether ACh signals in the sBG also convey information about syllable maturity, as shown for DA signals in the sBG (Fig. 2i–o). To resolve this issue, we expressed the ACh sensor GRAB-ACh3.0 in the sBG of previously tutored juvenile male zebra finches and recorded their songs while using fibre photometry to measure singing-related ACh transients in the sBG during sensorimotor learning (Fig. 4e). We further confirmed that singing-related ACh transients in the sBG of these juveniles were not observed with non-vocal movements (Extended Data Fig. 4k,l; $n = 5$ juvenile males). Unlike the DA signal, cross-correlation methods and LASSO-regularized regression analyses failed to detect a peak in the ACh signal that correlated with

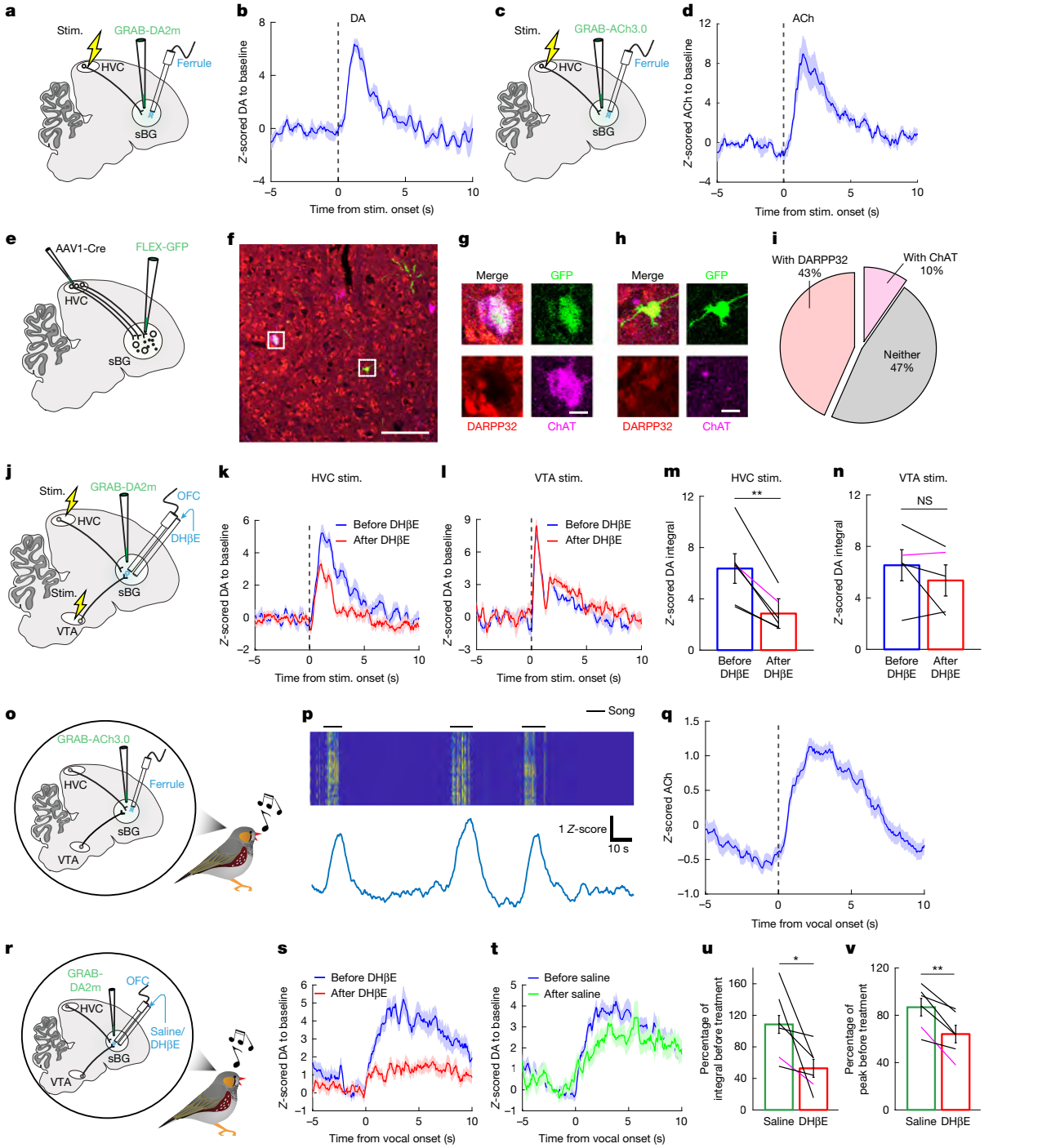


**Fig. 3 | Cholinergic-mediated DA release in the sBG. a**, Measuring DA evoked in the sBG by HVC stimulation. **b**, Mean DA evoked by HVC stimulation ($n = 6$ trials, one adult bird; replicated in 8 of 8 GRAB-DA adults). **c**, As in **a**, only for ACh. **d**, As in **b**, only for ACh ($n = 9$ trials, one adult bird; replicated in 7 of 7 GRAB-ACh adults). **e**, Intersectional viral strategy to identify sBG neurons receiving monosynaptic input from HVC. **f**–**h**, Low-power (**f**) and high-power (**g**,**h**, left (**g**) and right (**h**) boxes in **f**) images showing GFP (green) expression in ChAT$^+$ (magenta, cholinergic marker) or DARPP32$^+$ (red, spiny neuron marker) cells. **i**, Percentage of GFP$^+$ cells positive for ChAT (magenta), DARPP32 (red) and neither (grey) (83 GFP$^+$ neurons, 6 adults, 12 hemispheres). **j**, Measuring DHβE effects on HVC- or VTA-stimulated DA release in sBG. **k**,**l**, DA evoked in the sBG by HVC (**k**) and VTA (**l**). Stimulation before (blue, 12 trials in **k**, 6 trials in **l**) and after (red, 18 trials in **k**, 6 trials in **l**) infusing DHβE into the sBG. **m**, Areal difference between DA transients before or after infusing DHβE (0–2 s after stimulation, $n = 6$ adults, $t_5 = 5.038$, $P = 0.0040$, two-tailed paired $t$-test). **n**, As in **m** but after VTA stimulation ($n = 5$ adults, $t_4 = 1.393$, $P = 0.2360$, two-tailed paired $t$-test). Magenta lines in **m**,**n** are from examples in **k**,**l**. **o**, Singing-evoked ACh in the sBG. **p**, Representative ACh transients during song bouts. **q**, Singing-evoked ACh signal in the sBG aligned to song onset (54 trials, one adult bird, replicated in 6 of 6 adults). **r**, Singing-evoked DA before and after infusing DHβE. OFC, opto-fluid cannula. **s**, Singing-evoked DA transients in the sBG before (blue, 38 trials, one adult) and after (red, 41 trials, same bird) infusing DHβE. **t**, As in **s** but with saline (before, blue, 59 trials from bird in **s**; after, green, 33 trials from same bird). **u**, Percentage of areal change in singing-evoked DA transient, measured 0–5 s after song onset, after saline (green) or DHβE (red) infusion into the sBG ($n = 6$ adults, $t_5 = 2.764$, $P = 0.0396$, two-tailed paired $t$-test). **v**, Percentage change in peak singing-evoked DA transient after infusion of saline or DHβE, measured 0–5 s following song onset ($n = 6$ adults, $t_5 = 4.958$, $P = 0.0043$, two-tailed paired $t$-test). Magenta in **u**,**v** from examples in **s**,**t**. **b**,**d**,**k**,**l**,**q**,**s**,**t**, Solid trace, mean; shaded region, s.e.m. **m**,**n**,**u**,**v**, Boxes and error bars denote mean ± s.e.m. $^*P < 0.05$, $^{**}P < 0.01$, $^{***}P < 0.001$. Scale bars, 100 µm (**f**), 10 µm (**g**,**h**). NS, not significant.

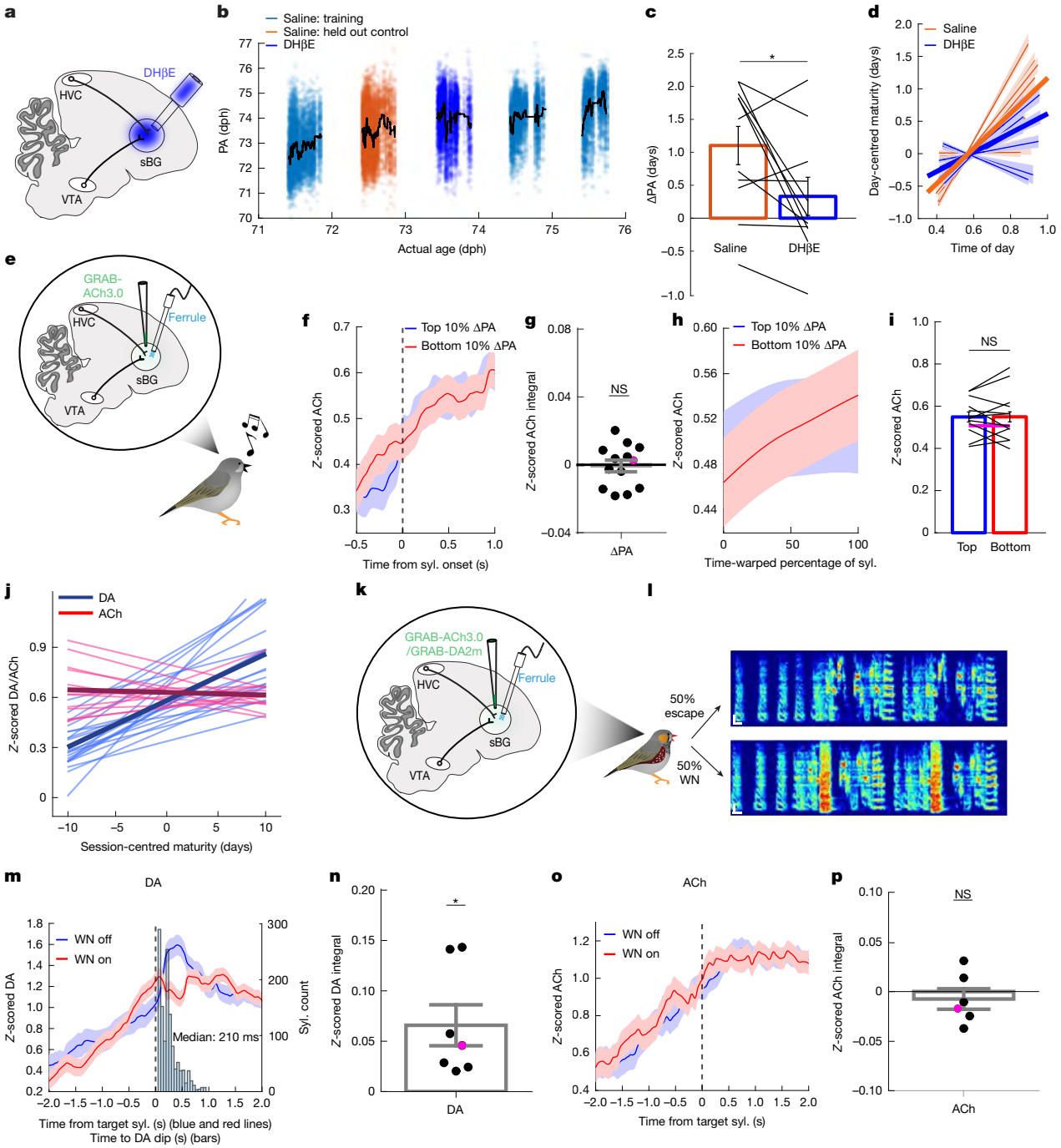


**Fig. 4 | DA and ACh contribute differently to song learning. a**, Reversibly blocking nAChRs in the sBG with DHβE. **b**, Predicted versus actual age for syllable renditions on saline days used to train the ANN (blue), saline control day (orange) and DHβE day (dark blue). Black, rolling average. **c**, Blocking nAChRs reduces daily syllable maturation (PA change, first 50 to last 50 renditions, $n = 11$ syllables, four juveniles; $t_{10} = 2.487$, $P = 0.0322$, two-tailed paired $t$-test). **d**, Blocking nAChRs reduced maturation across the day ($n = 11$ syllables, four juveniles; linear mixed-effects model, interaction between treatment (saline or DHβE) and time of day, $t_{50054} = -13.116$, $P = 3.0934 \times 10^{-39}$, two-tailed $t$-test). **e**, Measuring singing-evoked ACh in the sBG. **f**, Mean ACh transients for top (blue) and bottom (red) deciles of ΔPA renditions of an example syllable (529 per decile). **g**, Areal difference between the top or bottom mean ΔPA scores (0.1–0.3 s after syllable onset, 13 syllables, five juveniles; $t_{12} = 0.1478$, $P = 0.8849$, one-sample two-tailed $t$-test). Magenta dot, syllable in **f**. **h**, Time-warped ACh transients with 100-ms lag for top or bottom decile ΔPA renditions of syllable in **f**. **i**, Mean time-warped ACh transients for top or bottom decile ΔPA renditions (13 syllables, five juveniles; $t_{12} = 0.02838$, $P = 0.9778$, two-tailed paired $t$-test). Magenta line, syllable in **h**. **j**, Linear mixed-effects model showing correlation between ACh transients (red) and session-centred maturity (13 syllables, five juveniles, $\beta = -0.0016$, $t_{9.867} = -0.303$, $P = 0.768$, two-tailed $t$-test; DA data from Fig. 2o). **k**,**l**, Measuring effects of syllable-targeted white noise (**k**) (WN) on DA or ACh dynamics in sBG (**l**). **m**, Example DA transients in WN-on (red, 145 trials) and WN-off (blue, 98 trials) conditions. Time to first DA dip in WN-on trials, 210 ms after syllable onset; 1,275 renditions, seven birds. **n**, Areal difference between DA transients in sBG in WN-on and WN-off conditions (0.1–0.3 s after syllable onset, seven syllables, seven adults, $t_6 = 3.245$, $P = 0.0176$, one-sample two-tailed $t$-test). Magenta dot, example in **m**. **o**, Example ACh transients in WN-on (red, 99 trials) and WN-off (blue,103 trials) renditions. **p**, As in **n** but with ACh (six syllables, six adult birds, $t_5 = 0.7164$, $P = 0.5058$, one-sample two-tailed $t$-test). Magenta dot, example in **o**. **c**,**g**,**i**,**n**,**p**, Boxes and error bars, mean ± s.e.m. **f**,**h**,**m**,**o**, Solid trace, mean; shaded region, s.e.m. **d**, Dark lines, mean slope per group; light lines, posterior estimates for individual syllables; shaded regions, 95% confidence intervals. $^{*}P < 0.05$, $^{**}P < 0.01$, $^{***}P < 0.001$. Scale bars, 1 kHz (vertical), 50 ms (horizontal).

syllable maturity, even when accounting for other acoustic variables (Extended Data Fig. 4m–o). Applying a similar time window to that used for the DA analysis (100–300 ms after syllable onset), we then correlated these ACh signals with ΔPA and session-centred maturity scores. Neither analysis detected a significant relationship between the singing-related ACh transient in the sBG and syllable maturity (Fig. 4f–j; $n = 13$ syllables from five juvenile males). Additionally, an analysis of various syllable acoustic features showed that the magnitude of the ACh transient in the sBG positively correlated with syllable duration, similar to the DA signal and negatively correlated with mean frequency variance, as well as several other acoustic features (Extended Data Fig. 4p). However, none of these acoustic features correlated with rendition-to-rendition changes in syllable maturity, as captured by the ΔPA metric (Extended Data Fig. 4q).

These analyses show that the ACh and DA signals in the sBG convey different types of information during singing and indicate that only the DA signal encodes the learned quality of song performance. Because male zebra finches use hearing to assess their song performance, one way to probe this difference is to use syllable-triggered noise to interfere with singing-related auditory feedback[38]. Indeed, this approach has been used to show that the VTA DA neurons that innervate the sBG encode an RPE-like signal[22]. Therefore, we expressed either GRAB-DA2m or GRAB-ACh3.0 in the sBG of adult male zebra finches and delivered white noise bursts randomly on 50% of the renditions of a specific 'target' syllable in the bird's motif (Fig. 4k,l). Aligning fibre photometric recordings of DA signals to the onset of the target syllable showed that DA transients were significantly depressed on renditions 'hit' by noise, relative to 'escapes' (Fig. 4m,n; $n = 7$ syllables from seven adult males). The median of the time to the DA dip relative to the noise-targeted syllable onset was 210 ms, similar to a previous study[30] and in agreement with the temporal relationship between syllable onset and DA peaks associated with syllable maturity observed here (Fig. 2g,h). In contrast, the syllable-related ACh transient in the sBG did not differ between hit or escape renditions (Fig. 4o,p; $n = 6$ syllables from six adult males). Therefore, only the DA signal is sensitive to auditory feedback-dependent information that zebra finches use to assess the quality of song performance.

## Discussion

Here we show that rendition-to-rendition DA dynamics in the sBG track the learned quality of song performance during juvenile sensorimotor learning. Specifically, DA transients in the sBG were elevated when the juvenile produced renditions of a syllable that were relatively mature for its age and depressed when it produced relatively immature renditions, behaviour consistent with an RPE-like signal. As with DA signals associated with spontaneous behaviour[7], individual records are noisy and weak but gain coherence when averaged over many trials (Extended Data Fig. 2p,q). These DA dynamics tracked syllable maturity within several hundred milliseconds following syllable onset, consistent with performance-related fluctuations in VTA cell body firing[21] and DA transients recorded in the sBG in adult finches[30]. Although this combination of high noise and long feedback delays might at first seem inconsistent with behavioural learning at millisecond timescales, computational models nevertheless indicate that even weak, delayed correlations are sufficient to account for learning when averaged over thousands of syllable renditions[39,40]. In fact, we found that blocking neuronal activity or D1R-mediated signalling in the sBG largely prevented daily increases in syllable maturity (see also ref. 5), whereas previous studies showed that performance-contingent optogenetic manipulation of DA terminal activity in the sBG is sufficient to drive simpler forms of vocal learning in adult finches[5,23]. Therefore, the RPE-like DA dynamics in the sBG described here are not only necessary for sensorimotor learning—they are likely to guide it.

In addition to these performance-dependent DA dynamics, a noteworthy finding is that the DA signals in the sBG were always elevated above baseline levels during singing, regardless of song quality. We showed that much of this singing-related elevation in DA depends on song premotor activity transmitted from HVC that acts by means of nicotinic receptors in the sBG, similar to circuit mechanisms described in the mouse striatum[24–26]. This organization can help explain why the ACh and DA transients correlate with syllable duration, a feature controlled by HVC premotor activity[41], yet blocking nAChRs or D1Rs did not alter syllable duration. Furthermore, DA signals in the sBG correlate with acoustic features, including syllable duration and amplitude, that may signify song motor vigour. One possibility is that the correlations between DA and aspects of song motor vigour arise because more vigorous singing involves elevated premotor activity in HVC, which stimulates greater DA release through the ACh-dependent mechanism described here. However, although DA and ACh signals increase with song production, only DA provides an RPE-like signal that encodes the learned quality of song performance.

An important future goal will be to understand the broader significance of singing-related elevation of DA signals in the sBG. One possibility is that DA functions as an intrinsic reward to reinforce spontaneous singing, which is crucial for sensorimotor learning. Another possibility is that singing-related activity from HVC acts by means of cholinergic signalling in the sBG to elevate DA tone to levels that are optimal for learning. Unlike spiny neurons in the mouse striatum, many spiny neurons in the sBG express both D1 and D2 receptors[42,43], which bind DA with lower and higher affinity[44], and which couple to stimulatory and inhibitory G proteins, respectively. As the GRAB-DA sensor used here is engineered from the higher-affinity D2 receptor[27], the DA signals we detected in the sBG reflect higher-affinity DA receptor binding. Consequently, the tonic, singing-dependent elevation of DA in the sBG driven by HVC may more completely occupy D2 receptors while leaving D1Rs less occupied. This arrangement could enable performance-dependent fluctuations in DA release from VTA terminals to bidirectionally modulate cAMP levels in SNs that express both D1 and D2 receptors. This in turn would allow the same SNs to contribute to both positive and negative reinforcement of song motor programs, a feature of VTA-dependent DA signalling in the sBG[23,45].

Beyond showing that singing-related DA transients in the sBG depend partly on ACh signalling, the present study also shows that these two neuromodulators have distinct roles in sensorimotor learning: whereas blocking either D1 or nAChRs in the sBG impaired daily learning, only the DA signal acutely and reliably tracked the rendition-to-rendition fluctuations in syllable maturity. Finally, the DA signal in the sBG was sensitive to noise perturbation of singing-related auditory feedback (see also ref. 30), as has been shown for the action potential activity of VTA cell bodies that innervate the sBG[22]. By comparison, feedback perturbations had no effect on ACh signals in the sBG (shown here) and do not alter the singing-related action potential activity of the HVC neurons that provide input to the sBG[36,46]. These findings support a mechanism where HVC song premotor activity transmitted to the sBG tonically elevates ACh and DA during song production, whereas the VTA drives phasic DA fluctuations that encode and reinforce the learned features of song performance.

## Online content

Any methods, additional references, Nature Portfolio reporting summaries, source data, extended data, supplementary information, acknowledgements, peer review information; details of author contributions and competing interests; and statements of data and code availability are available at https://doi.org/10.1038/s41586-025-08694-9.


1. Schultz, W., Dayan, P. & Montague, P. R. A neural substrate of prediction and reward. *Science* **275**, 1593–1599 (1997).
2. Gershman, S. J. & Uchida, N. Believing in dopamine. *Nat. Rev. Neurosci.* https://doi.org/10.1038/s41583-019-0220-7 (2019).

3. Wood, A. N. New roles for dopamine in motor skill acquisition: lessons from primates, rodents, and songbirds. *J. Neurophysiol.* **125**, 2361–2374 (2021).
4. Blain, B. & Sharot, T. Intrinsic reward: potential cognitive and neural mechanisms. *Curr. Opin. Behav. Sci.* **39**, 113–118 (2021).
5. Hisey, E., Kearney, M. G. & Mooney, R. A common neural circuit mechanism for internally guided and externally reinforced forms of motor learning. *Nat. Neurosci.* **21**, 589–597 (2018).
6. Thorndike, E. L. *The Elements of Psychology* (Seiler, 1905).
7. Markowitz, J. E. et al. Spontaneous behaviour is structured by reinforcement without explicit reward. *Nature* **614**, 108–117 (2023).
8. Doupe, A. J. & Kuhl, P. K. Birdsong and human speech: common themes and mechanisms. *Annu. Rev. Neurosci.* **22**, 567–631 (1999).
9. Sakata, J. T., Woolley, S. C., Fay, R. R. & Popper, A. N. *The Neuroethology of Birdsong* (Springer Nature, 2020).
10. Mooney, R. Birdsong. *Curr. Biol.* **32**, R1090–R1094 (2022).
11. Derégnaucourt, S., Mitra, P. P., Fehér, O., Pytte, C. & Tchernichovski, O. How sleep affects the developmental learning of bird song. *Nature* **433**, 710–716 (2005).
12. Goffinet, J., Brudner, S., Mooney, R. & Pearson, J. Low-dimensional learned feature spaces quantify individual and group differences in vocal repertoires. *eLife* **10**, e67855 (2021).
13. Brudner, S., Pearson, J. & Mooney, R. Generative models of birdsong learning link circadian fluctuations in song variability to changes in performance. *PLoS Comput. Biol.* **19**, e1011051 (2023).
14. Eales, L. A. Song learning in zebra finches: some effects of song model availability on what is learnt and when. *Anim. Behav.* **33**, 1293–1300 (1985).
15. Price, P. H. Developmental determinants of structure in zebra finch song. *J. Comp. Physiol. Psychol.* **93**, 260–277 (1979).
16. Singh Alvarado, J. et al. Neural dynamics underlying birdsong practice and performance. *Nature* **599**, 635–639 (2021).
17. Person, A. L., Gale, S. D., Farries, M. A. & Perkel, D. J. Organization of the songbird basal ganglia, including area X. *J. Comp. Neurol.* **508**, 840–866 (2008).
18. Feenders, G. et al. Molecular mapping of movement-associated areas in the avian brain: a motor theory for vocal learning origin. *PLoS ONE* **3**, e1768 (2008).
19. Doya, K. & Sejnowski, T. A novel reinforcement model of birdsong vocalization learning. In *Proc. Advances in Neural Information Processing Systems* Vol. 7 (eds Tesauro, G. et al.) 101–108 (MIT, 1994).
20. Fee, M. S. & Goldberg, J. H. A hypothesis for basal ganglia-dependent reinforcement learning in the songbird. *Neuroscience* **198**, 152–170 (2011).
21. Duffy, A., Latimer, K. W., Goldberg, J. H., Fairhall, A. L. & Gadagkar, V. Dopamine neurons evaluate natural fluctuations in performance quality. *Cell Rep* **38**, 110574 (2022).
22. Gadagkar, V. et al. Dopamine neurons encode performance error in singing birds. *Science* **354**, 1278–1282 (2016).
23. Xiao, L. et al. A basal ganglia circuit sufficient to guide birdsong learning. *Neuron* **98**, 208–221.e5 (2018).
24. Mohebi, A., Collins, V. L. & Berke, J. D. Accumbens cholinergic interneurons dynamically promote dopamine release and enable motivation. *eLife* **12**, e85011 (2023).
25. Liu, C. et al. An action potential initiation mechanism in distal axons for the control of dopamine release. *Science* https://doi.org/10.1126/science.abn0532 (2022).
26. Kramer, P. F. et al. Synaptic-like axo-axonal transmission from striatal cholinergic interneurons onto dopaminergic fibers. *Neuron* **110**, 2949–2960.e4 (2022).
27. Sun, F. et al. Next-generation GRAB sensors for monitoring dopaminergic activity in vivo. *Nat. Methods* **17**, 1156–1166 (2020).
28. Ko, D. & Wanat, M. J. Phasic dopamine transmission reflects initiation vigor and exerted effort in an action- and region-specific manner. *J. Neurosci.* **36**, 2202–2211 (2016).
29. Panigrahi, B. et al. Dopamine is required for the neural representation and control of movement vigor. *Cell* **162**, 1418–1430 (2015).
30. Roeser, A. et al. Dopaminergic error signals retune to social feedback during courtship. *Nature* **623**, 375–380 (2023).
31. Bottjer, S. W., Halsema, K. A., Brown, S. A. & Miesner, E. A. Axonal connections of a forebrain nucleus involved with vocal learning in zebra finches. *J. Comp. Neurol.* **279**, 312–326 (1989).
32. Chantranupong, L. et al. Dopamine and glutamate regulate striatal acetylcholine in decision-making. *Nature* **621**, 577–585 (2023).
33. Krok, A. C. et al. Intrinsic dopamine and acetylcholine dynamics in the striatum of mice. *Nature* **621**, 543–549 (2023).
34. Jing, M. et al. An optimized acetylcholine sensor for monitoring in vivo cholinergic activity. *Nat. Methods* **17**, 1139–1146 (2020).
35. Zingg, B. et al. AAV-mediated anterograde transsynaptic tagging: mapping corticocollicular input-defined neural pathways for defense behaviors. *Neuron* **93**, 33–47 (2017).
36. Kozhevnikov, A. A. & Fee, M. S. Singing-related activity of identified HVC neurons in the zebra finch. *J. Neurophysiol.* **97**, 4271–4283 (2007).
37. Goldberg, J. H. & Fee, M. S. Singing-related neural activity distinguishes four classes of putative striatal neurons in the songbird basal ganglia. *J. Neurophysiol.* **103**, 2002–2014 (2010).
38. Tumer, E. C. & Brainard, M. S. Performance variability enables adaptive plasticity of 'crystallized' adult birdsong. *Nature* **450**, 1240–1244 (2007).
39. Fiete, I. R., Fee, M. S. & Seung, H. S. Model of birdsong learning based on gradient estimation by dynamic perturbation of neural conductances. *J. Neurophysiol.* **98**, 2038–2057 (2007).
40. Farries, M. A. & Fairhall, A. L. Reinforcement learning with modulated spike timing dependent synaptic plasticity. *J. Neurophysiol.* **98**, 3648–3665 (2007).
41. Long, M. A. & Fee, M. S. Using temperature to analyse temporal dynamics in the songbird motor pathway. *Nature* **456**, 189–194 (2008).
42. Ding, L. & Perkel, D. J. Dopamine modulates excitability of spiny neurons in the avian basal ganglia. *J. Neurosci.* **22**, 5210–5218 (2002).
43. Kubikova, L., Wada, K. & Jarvis, E. D. Dopamine receptors in a songbird brain. *J. Comp. Neurol.* **518**, 741–769 (2010).
44. Richfield, E. K., Penney, J. B. & Young, A. B. Anatomical and affinity state comparisons between dopamine D1 and D2 receptors in the rat central nervous system. *Neuroscience* **30**, 767–777 (1989).
45. Kearney, M. G., Warren, T. L., Hisey, E., Qi, J. & Mooney, R. Discrete evaluative and premotor circuits enable vocal learning in songbirds. *Neuron* **104**, 559–575.e6 (2019).
46. Hamaguchi, K., Tschida, K. A., Yoon, I., Donald, B. R. & Mooney, R. Auditory synapses to song premotor neurons are gated off during vocalization in zebra finches. *eLife* **3**, e01833 (2014).


**Publisher's note** Springer Nature remains neutral with regard to jurisdictional claims in published maps and institutional affiliations.

Springer Nature or its licensor (e.g. a society or other partner) holds exclusive rights to this article under a publishing agreement with the author(s) or other rightsholder(s); author self-archiving of the accepted manuscript version of this article is solely governed by the terms of such publishing agreement and applicable law.

© The Author(s), under exclusive licence to Springer Nature Limited 2025, corrected publication 2025

# Methods

### Animals

Juvenile (31–95 dph) and adult (120–667 dph) male zebra finches (*Taeniopygia guttata*) were obtained from the Mooney Lab breeding colony from Duke University Medical Center animal facility. Birds were kept under a 14:10-h light:dark cycle with free access to food and water. All experiments were performed under a protocol approved by Duke University Institutional Animal Care and Use Committee. A summary of birds used in this study is in Extended Data Table 1.

### General surgery

Male zebra finches were anaesthetized with 2% isoflurane before being head-fixed on a stereotaxic apparatus with a heat pad. The rate of breathing was monitored throughout surgery. After trimming the feathers over the skull, applying 0.25% bupivacaine as a topical anaesthetic and three rounds each of betadine and 70% ethanol, a vertical incision was made with a scalpel in the skin from anterior to posterior. Craniotomies were made according to the stereotaxic coordinates of specific brain regions, which were used to localize target sites for injection, implantation and electric stimulation. Stereotaxic coordinates measured from the posterior edge of the bifurcation of the midsagittal sinus (Y-sinus): for HVC, head angle 18°, 0.0 mm rostral, 2.4 mm lateral and 0.4 mm ventral; for VTA, head angle 37°, 1.65 mm rostral, 0.5–1.5 mm lateral, 6.2 mm ventral; for sBG, head angle 43°, 5.1 mm rostral, make a mark, switch to head angle 72°, 1.7 mm rostral from mark, 1.6 mm lateral, 3.1–2.6 mm ventral (this coordinate avoids damaging LMAN). RetroBeads or viruses (specified below for each experiment) were injected using a glass pipette attached to a Nanoject-II or Nanoject-III (Drummond Scientific). After injections, craniotomies were closed with the original piece of skull, and the incision site in the scalp was closed with either a tissue adhesive (Vetbond) or suture. Zebra finches were monitored in a recovery cage with food and water under a heat lamp until fully recovered before the bird was returned to the bird colony or a sound isolation box for further experiments.

### Microdialysis experiments

Microdialysis probes were made in house with polyethylene tubing (Intramedic, 427406) thatserved as a drug reservoir, a guide tube (MicroLumen, 4550698947), an outflow tube (MicroLumen, 4550814963) and a permeable tube (Spectra/Por, 132294), which allowed the drug to slowly diffuse throughout the day. For probe design, see ref. 47. Juvenile zebra finches were raised in the company of an adult male tutor until 55–60 dph. Using the surgical procedures and stereotaxic coordinates described above, craniotomies were made over the sBG. Probes were then implanted bilaterally, with the tip of the permeable membrane placed at the most ventral part of the sBG so that the permeable membrane extended through the dorsoventral span of the sBG. The surgical site was covered with a silicone adhesive, KWIK-SIL (WPI), and the probes were secured in place using MetaBond (Parkell, S396, S398, S371). For the DHβE infusion group, AAV2/9-CAG-GFP (Addgene, 37825-AAV9) was injected bilaterally to HVC before probe implantation to label HVC terminals in the sBG. After recovery, birds were placed in a sound isolation box and left for two to three days until their singing rate recovered to normal levels.

For data acquisition, songs were automatically recorded with Sound Analysis Pro (SAP; http://soundanalysispro.com/). All infusions were done 5–15 min before cage lights came on every morning. For the infusion schedule, 4–6 days of saline were recorded as baseline learning days, followed by one day of drug. Drugs were washed out the next morning before lights came on, followed by at least 4 days of saline. For the muscimol experiment ($n$ = 5 of 15 microdialysis birds), muscimol was given 6 days after birds had received a previous drug treatment, and analysis was restricted to a window around muscimol treatment. In all other birds ($n$ = 10 of 15), we reported data from the first drug treatment. The following concentrations and drugs were used for the microdialysis experiments: muscimol (750 μM, Tocris, 0289), SCH-23390 (5 mM, Tocris, 0925), DHβE (5 mMM Tocris, 2349). All drugs were prepared in a mammalian Ringer's solution (Electron Microscopy Science, 11763-10). At the end of data collection, a fluorescent dye, Fast Green (1 mg ml$^{-1}$, Sigma, F7252), was infused through the microdialysis probes to visualize drug spread. Birds were perfused with fixative, and brains were collected and sectioned to confirm probe localization.

### VAE

After recording a large corpus of a juvenile's songs during a period that spanned much of sensorimotor learning (55–94 dph), individual song renditions were segmented into their component syllables using the Autoencoded Vocal Analysis (AVA) package in Python[12]. Briefly, spectrograms were taken as the log modulus of a short time Fourier transform (Hann windows; sample rate, 44.1 kHz; segment length, 512; overlap, 320). The total power of the spectrogram was calculated across channels. Syllables were detected when the total power exceeded a threshold, manually chosen for each bird. Detected syllables were then manually scaled and clipped to an appropriate range. They were interpolated to 128 target frequencies linearly spaced between 300 and 8,000 Hz and 128 target times, resulting in a 128 × 128 spectrogram. After VAE training, syllables were labelled according to the UMAP projections of embedded spectrograms using custom software in MATLAB.

We used a standard VAE model to encode spectrograms, trained separately for each bird. VAEs embed data ($X$) into a low-dimensional compressed representation ($Z$) through an encoder distribution ($q_\phi(Z|X)$, with parameters $\Phi$) and then try to reconstruct the original data from this latent space using a decoder distribution ($p_\theta(X|Z)$, with parameters $\theta$). The model is trained by minimizing the following objective:

$$\mathcal{L}(X;\theta,\Phi) = -E_{q_\phi(Z|X)}[\log p_\theta(X|Z)] + \mathrm{KL}(q_\phi(Z|X)|p(Z))$$

The first term encourages high-fidelity reconstruction of the original data, and the second, involving a Kullback–Leibler divergence, pulls the embedding towards a simple prior distribution. We used a standard Gaussian prior. The latent dimension was fixed at 32 with the same deep convolutional neural network architecture used as in a previous study[13]. All parameters were optimized using Adam optimization with a learning rate of 0.001. Eighty per cent of the syllables were used for training, and the remaining 20% were set aside for VAE validation. We trained the model until loss stopped decreasing on the validation set (150–350 epochs). To assess variability in the latent space after drug treatment, we calculated the mean rendition in latent space for a given day (32 values), calculated the distance between each rendition and that mean in latent space, and then calculated the average distance to measure dispersion from the mean. We then normalized this distance in the drug day relative to the preceding vehicle injection day (treatment/vehicle × 100%, Extended Data Figs. 1l,q and 4h).

### ANN for PA

Once the VAE was fully trained and syllables were segmented, we extracted latent embeddings for each syllable. We then trained a separate ANN with 3 linear layers to predict the age at which each syllable was produced, using a previously described approach[13]. For drug treatment experiments, we restricted ANN training to a narrower developmental window that bracketed this drug treatment day (2–4 days before and after drug treatment day). Specially, both the drug day and the previous saline day were held out of the training set. During training, syllable ages were scaled between −1 and 1 independently for each syllable. All network parameters were optimized by minimizing the sum of squared errors between predicted and actual age, using the Levenberg–Marquardt algorithm with Bayesian regularization. Briefly, this method of training trades off between prediction error and network complexity, biasing learning towards simpler networks with smooth

responses[48]. As when training the VAE, 80% of the syllables were used for training and the remaining 20% were set aside for model validation. We trained for a maximum of 30 min and terminated a run if there was no improvement on the validation set objective for three epochs. After obtaining PA for each syllable, we compared the change in PA from the first 50 to the last 50 renditions of a syllable in the drug day and the previous saline day to see the effect of drug treatment (Figs. 1i,m and 4c). Normalized learning rate was calculated by dividing the ΔPA over drug day and saline day by total syllable renditions produced on the day (Extended Data Figs. 1e,g and 4c). Day-centred maturity was calculated by subtracting PA from the mean PA of the drug treatment day or the previous saline control day (Figs. 1j,n and 4d). For each syllable, we defined two measures of maturity: ΔPA and session-centred maturity. ΔPA was calculated as the change in PA between successive renditions of the same syllable. Session-centred maturity was the PA of each syllable mean-centred to the average PA of that same syllable for a single recording session.

### Linear mixed-effects models

Linear mixed-effects models allowed us to account for covariance structure related to hierarchical relationships in our data while modelling population-level effects. Specifically, we accounted for correlations between measurements that were sampled from the same bird by including random effect terms for each type of measurement. In analyses relating DA and ACh to song maturity (Figs. 2o and 4j), our outcome variable was the average DA (or ACh) from 100 to 300 ms after syllable onset. We fit either session-centred maturity or ΔPA as fixed effects and added recording session (grouped by syllable type) and syllable type (grouped by bird) as random effects. In analyses relating time of day to song maturity, separated by drug treatment (Figs. 1j,n and 4d), our outcome variable was day-centred maturity. We fit fixed effects of time of day, drug (treatment or control) and interaction between the two. We added random effects of syllable ID (grouped by bird) and bird. In analyses relating the treatment's effect on song duration (ringers versus DHβE, Extended Data Table 2), our outcome variable was song duration. We fit fixed effects of treatment time (before or after treatment), treatment type (DHβE or control) and interaction. We added a random effect of bird. Mixed-effects models were fitted using lme4 (ref. 49) and MATLAB (Mathworks).

### LASSO-regularized linear models

We used LASSO-regularized linear models[50] to select variables that contributed distinct information to DA and ACh signals. All predictors (SAP parameters and ΔPA) were *Z*-scored to session mean and s.d. separately for each syllable before model fitting, such that all parameters for all syllables had a comparable numerical range and regularization would have the same effect on each. These models minimize mean-squared error between outcomes ($y$) and predictions ($X$) while penalizing the sum of absolute values of their parameters ($\beta$) using a regularization weight ($\lambda$):

$$\mathcal{L}(\beta) = \mathrm{E}[(y - X^T\beta)^2] + \lambda \sum_{i=1}^{P} |\beta_i|$$

This optimization forces parameters for variables that do not provide significant information about outcomes to zero. Our outcome variable was mean DA (or ACh) from 100 to 300 ms after syllable onset. Our predictors were either session-centred maturity or ΔPA and all acoustic features. We selected an optimal value of $\lambda$ using 10-fold cross-validation, picking the largest $\lambda$ such that mean-squared error was within one standard error of the minimum. LASSO-regularized linear models were fitted using glmnet (R)[51].

### Song feature analysis

To quantify the acoustic features of syllables, we first used the AVA–VAE segmentation decisions to segment song files into individual files for each rendition of each syllable. We then used the batch analysis capability of Sound Analysis Pro v.2011.104 (http://soundanalysispro.com/) to quantify a set of standard acoustic features for each rendition of each syllable. These data were saved into an excel file and subsequently loaded into MATLAB for analysis using custom scripts. In the case of assessing how microdialysis manipulations (muscimol, SCH-23390 or DHβE) influenced acoustic features, we calculated the mean and s.d. of each feature on both the vehicle pretreatment day and the drug treatment day. We also calculated the coefficient of variation of pitch as (standard deviation/mean) × 100%. We then calculated a change in baseline for the mean and s.d. of each acoustic feature as follows: (treatment/vehicle) × 100%. We then tested for significant differences from 100% using one-sample *t*-tests, which were Bonferroni-corrected for several comparisons. We used these same normalized to vehicle values for the coefficient of variation of pitch and mean frequency modulation following DHβE treatment and performed linear regressions relating these features to changes in maturity to determine if DHβE might attenuate increases in maturity through altering these features.

When assessing how DA and ACh transients correlated with acoustic features, we used custom MATLAB scripts to align the acoustic feature data with the DA (or ACh) signal 100–300 ms after the onset of each syllable rendition. We then found the top and bottom 10% for each individual acoustic feature in each day and calculated the average DA (or ACh) signal for the top or bottom decile of each acoustic feature. A two-way RM ANOVA with post hoc Bonferroni-corrected multiple comparisons was used to determine if there was a significant difference in DA (or ACh) transients related to any individual acoustic feature. We also calculated Pearson correlations between individual acoustic features and ΔPA to determine if they were independent of one another.

### Fibre photometry

Adult or juvenile male zebra finches were injected with AAV2/9-hSyn-GRAB_DA2m (WZ Biosciences, YL002009-AV9-PUB), AAV2/9-hSyn-GRAB_ACh3.0 (WZ Biosciences, YL001003-AV9-PUB) or AAV2/9-CAG-GFP (Addgene, 37825-AAV9) into the sBG using the procedure described in 'General surgery'. Specifically, viruses were injected at three different ventral coordinates per hemisphere (3.1, 2.8, 2.6 mm, 300 nl for each site) in the sBG. Fibre-optic ferrules were implanted unilaterally (counterbalanced for hemisphere) during the same surgery as the viral injection. Craniotomies were made over the sBG and fibre-optic ferrules (200 μm core, 0.37 NA, Neurophotometrics) were implanted to the dorsal edge of sBG (2.6 mm ventral). For simultaneous photometry recording and pharmacology manipulation, opto-fluid cannulae (Doric Lenses) were implanted unilaterally (counterbalanced for hemisphere) after waiting a minimum of 3 weeks for viral expression and secured in place using MetaBond. Fibre placement was verified in brain sections at the end of the experiment.

For data acquisition, at least 3 weeks after optic ferrule implantation or 2–3 days after opto-fluid cannula implantation, birds were attached to a photometry system (Neurophotometrics FP3002) through a patch cord (Doric Lenses, 200 μm core, 0.37 NA). In brief, light from 470-nm-channel (for imaging in green fluorescence) and 415-nm-channel (for isosbestic control signal to detect motion artefacts) LEDs was generated in turn at a total frame rate of 30 Hz (15 Hz per wavelength), bandpass filtered and directed down the patch cord by means of a ×20 objective. Because the system is LED based, excitation spectra is a band in the following range for each LED: 415 nm LED, 400–425 nm; 470 nm LED, 445–486 nm. Light was measured at the tip of the patch cord to make sure the power for each wavelength was about 50 μW. Emitted GRAB-DA/ACh/GFP fluorescence was collected through the same cannula and patch cord, split by a dichroic mirror, bandpass filtered and focused onto opposite sides of an sCMOS camera sensor. The spectral range for the green emission channel was 494–531 nm. Data were acquired using the open-source software Bonsai[52] by drawing a

region of interest inside the green image of the patch cord and calculating the mean pixel value. Synchronized video and sound recordings were acquired using a webcam (Logitech).

Photometry data were analysed using custom-written MATLAB scripts. In each imaging session, the blue channel was fitted to and subtracted from the green signal using the MATLAB polyfit function. DA, ACh and GFP signals were *Z*-scored in each imaging session and aligned to the audio recordings. In electric stimulation and DHβE opto-fluid cannula experiments, *Z*-score to baseline was used instead of *Z*-score to the whole imaging session. Baseline was defined as 4–2 s before stimulation onset and 2–1 s before vocal onset.

For the juvenile DA experiment, AAV2/9-GRAB-DA2m was injected into the sBG between 33 and 38 dph for five juvenile males. Each juvenile was housed with an adult male tutor until 55–60 dph. One to nineteen 5- to 10-min fibre photometry sessions were made across each day for a 11.0 ± 4.7-day (mean ± s.d.) window between 63 and 90 dph). For the juvenile ACh experiment, AAV2/9-GRAB-ACh3.0 was injected into the sBG between 38 and 45 dph for five juvenile males. One to nine, 5 to 10-minute fibre photometry sessions were made across the day for a 11.6 ± 3.0 day (mean ± s.d.) window between 57 and 80 dph. After data collection, songs were fed into the VAE–ANN to generate PA scores for each syllable. ΔPA was calculated as the change in PA between successive renditions of the same syllable. The top and bottom 10% of ΔPA trials were selected for each day, and DA and ACh signals were aligned to syllable onsets. For the analysis in Figs. 2k and 4h, syllables were interpolated to the same length (16 samples). Session-centred maturity was calculated as the PA mean-centred in each 5-min imaging session.

For the electrical stimulation experiment, birds with a previously implanted optic ferrule or opto-fluid cannula were anaesthetized with 2% isoflurane and placed in a stereotaxic apparatus. A pulse train (20 Hz, 1 ms on, 49 ms off, for 1 s) was generated by a custom-written LabView function (National Instruments) and 200-400-μA current was delivered through a bipolar stimulating electrode (MicroProbes for Life Science, WE5ST30.1H10) to stimulate the target brain region. Electrode placement was confirmed post hoc in brain sections using DiI (Invitrogen, V22889) and/or the lesion caused by the electrode barrel. Fluorescence signal was captured by an FP3002 (Neurophotometrics) and a collateral of the pulse train was fed into the FP3002 for signal alignment. For experiments that measured the effects of DHβE on stimulation-evoked DA transients, a total of 3–8 stimulated trials conducted at 10–20-min intervals were used to calculate the mean baseline stimulation-evoked GRAB-DA transient before manually infusing 1 μl 5 mM DHβE through the cannula. After waiting at least 5 min for drug diffusion, the GRAB-DA transients evoked by 3–8 stimulated trials conducted at 10–20-min intervals were used to compare with baseline response. For experiments that measured the effects of scopolamine on the HVC-evoked ACh transient, the mean baseline GRAB-ACh transient was calculated from 3–5 stimulation trials conducted at 10-min intervals using the stimulus parameters mentioned above, with the current amplitude at 200 μA. Then, one ($n = 3$) or two ($n = 2$) injections of 5–20 mg kg$^{-1}$ body weight scopolamine (Tocris, 1414) dissolved in 0.9% saline were administered intramuscularly, and stimulus-evoked GRAB-ACh transients were measured at 10-min intervals for 1–4 h following the injection. The mean evoked response was calculated from 3–4 stimulation trials 15–60 min after the last injection and compared to the mean baseline response.

For the simultaneous pharmacology and photometry recordings, an injector containing saline or 1–5 mM DHβE was plugged into the opto-fluid cannula at about 10 a.m. Photometry recordings were collected with the FP3002 for several 5-min sessions until the middle of the day. At about 1:30 p.m., 1 μl 1–5 mM DHβE/saline was manually infused into the brain. After waiting at least 5 min for drug diffusion, several photometry recordings were collected until the injector was removed from the opto-fluid cannula at about 5 p.m. Probe placement was confirmed post hoc.

### Analysis of temporal correlation between DA/ACh and syllable maturity, amplitude and duration

To determine the optimal time window for our DA analyses, we used cross-correlation and LASSO-regularized regression across time (Fig. 2g,h and Extended Data Fig. 4m,n). For each of these methods, we turned session-centred maturity into a time series, mirroring the DA signal (or ACh). This maturity time series consisted of zeros everywhere except syllable onsets, where its value was the session-centred maturity of the syllable. We similarly transformed syllable amplitude and duration into time series.

For our cross-correlation analysis, we took 2-s windows of DA (or ACh) and maturity, centred at syllable onset, and calculated the average time-lagged cross-correlation across renditions between these two time series for each syllable. We performed this same cross-correlation between syllable duration and DA and syllable amplitude and DA. We likewise performed a regression analysis to estimate the convolutional kernel that would best predict DA (or ACh) from the maturity time series. More specifically, we sought to predict measured DA at the centre of a 2-s sliding window using the maturity time series over that same period. Windows began at the onset of the first syllable preceded by at least 2 s of silence and were slid forward in time until there was a gap of at least 2 s until the next syllable onset. We fit the kernel by minimizing the mean-squared error between predicted and true DA. We additionally used LASSO regularization to ensure that each only time lags where maturity could predict DA would have non-zero coefficients.

### DA heatmap analysis

For the heatmaps of DA traces for the top and bottom 5% ΔPA renditions (Extended Data Fig. 2r), we aligned DA to syllable onset. To baseline each trace, we subtracted an exponential moving average of all previous traces, defined as

$$\hat{X}_t = \alpha X_t + (1-\alpha)\hat{X}_{t-1}$$

$X_t$ indicates the DA recorded at time $t$ and $0 < \alpha < 1$ is a smoothing parameter. We used $\alpha = 0.8$, such that the 'baseline' DA for each rendition was effectively a weighted average of the previous five renditions.

### Video analyses

During photometry recording, the bird's position was recorded at 24 frames per second using a logitech webcam. For each juvenile DA and ACh bird, one 5-min recording session was randomly selected for locomotion analysis. ezTrack[53] was used to detect and track the centroid of the body position across video frames. Speed of movement was calculated as the change in position across pairs of frames. Acceleration of movement was calculated as the change in speed across pairs of frames. We found peaks in this acceleration data and then selected only the top 10% of peaks, which were also separated from adjacent peaks by at least three frames. These peaks were designated as movement onsets (Extended Data Figs. 2g,h and 4k,l).

### Syllable-targeted white noise experiment

Birds' songs were recorded, and a template to detect the fundamental frequency (that is, pitch) of a tonal syllable was made in a custom software program (EvTAF)[38]. The template was designed to detect at least 75% of the renditions of the targeted syllable with no more than 10 ms jitter in detection onset. The template was used to trigger a 50-ms white noise burst (about 70 dB) through a nearby speaker to the bird about a random 50% of times when the template detected that targeted syllable. DA (or ACh) signals were aligned to the onset of target syllable in white noise

hit and escape trials (Fig. 4m–p). For the analysis of time to the first DA dip during WN-hit trials (Fig. 4m), we identified 1,275 syllable renditions from seven birds; events shorter than 50 ms were excluded.

### Correlation analyses

We assessed the independence of vocal maturity across different syllables using a correlation analysis (Extended Data Fig. 2i,j). In each recording session, we mean-centred PA independently for each syllable. We then calculated the Pearson correlation between the maturities of successive syllables (for example, corr(AB), corr(BC), corr(CD) and so on). This true correlation was then compared to an empirical null distribution obtained through bootstrapped permutation. Briefly, we shuffled syllable labels between each pair within session and recalculated correlations 10,000 times per session–syllable pair. Pairs were considered to have significant correlation if their true correlation fell above 97.5% of the permuted correlation values or below 2.5% of the permuted correlation values.

We additionally looked for correlations on longer timescales by autocorrelating mean-centred maturity across each session at different lags (Extended Data Fig. 2k,l). We calculated this lagged autocorrelation using all syllables to assess independence of vocal maturity across all different syllables. We also calculated lagged autocorrelation separately for each syllable to assess the independence of vocal maturity across renditions of the same syllable. In each of these cases, we compared the empirical autocorrelation to the autocorrelation of independent, identically distributed samples of mean-zero Gaussian white noise, which has no autocorrelation structure.

To assess the relationship between maturity measures and acoustic features, we correlated maturity with acoustic features separately for each bird. We calculated correlation on each recording day.

### Tissue collection

Birds were deeply anaesthetized with intramuscular injection of 20 µl Euthasol (Virbac) and transcardially perfused with 1× phosphate-buffered saline (PBS, Sigma, P5493) followed by 4% paraformaldehyde (PFA). Brains were removed, post-fixed in 4% PFA at 4 °C overnight and moved to cryoprotective 30% sucrose PFA solution at 4 °C for 2 days. Brains were then frozen in Tissue-Tek OCT Compound (VWR, 25608-930) in disposable embedding moulds (VWR, 15160-157) and stored at −80 °C until sectioning. Frozen consecutive sagittal sections (thickness of 50 µm) were collected with a Leica CM 1850 cryostat and stored in 1× PBS solution at 4 °C until further procedures. For in situ hybridization, RNase-free PBS was prepared using 1× PBS (Invitrogen, AM9624) treated with DEPC (Sigma, D5758) and was used in these procedures.

### Immunofluorescence

Free-floating sections were washed for 5 min three times in 0.3% Triton X-100 (Sigma, T8787) in 1× PBS (0.3% PBST), blocked with 10% Blocking One Histo (Nacalai tesque, 06349-64) in PBST for 1 h and incubated with primary antibodies in PBST at 4 °C overnight. Sections were then washed for 5 min three times in PBST and incubated with secondary antibodies and Neurotrace 435/455 (1:500, Invitrogen, N21479) at room temperature for 4 h, followed by three 5-min washes in PBST. Sections were coverslipped with Fluoromount-G (SouthernBiotech, 0100-01) and then imaged with a confocal microscope (Zeiss 710) for single-plane or *Z*-stack images, as needed. ImageJ with Fiji (v.1.51s, https://imagej.net/software/fiji/) was used for image analysis.

For identification of microdialysis probes (Extended Data Fig. 1c) and electrode in HVC (Extended Data Fig. 3a), sections were directly incubated in Neurotrace 435/455 for 2 h while skipping the procedures on day 1. For identification of GRAB-DA2m (Extended Data Fig. 2a), GRAB-ACh3.0 (Extended Data Fig. 3e) and HVC terminals (Extended Data Fig. 4a) in the sBG, the combination of antibodies was used as follows: mouse anti-GFP (1:500, Invitrogen, A11120) and goat anti-mouse Alexa Fluor 488 (1:500, Invitrogen A11001). For identification of electrode placement in VTA (Extended Data Fig. 2b), the following antibodies were used: rabbit anti-tyrosine hydroxylase (1:1000, Millipore, AB152), goat anti-rabbit 488 (1:500, Invitrogen, A11034). For identification of ChAT, DARPP32 and GFP in Fig. 3f–h and Extended Data Fig. 3i, the following combination of antibodies was used: mouse anti-GFP (1:500, Invitrogen, A11120) and donkey anti-mouse Alexa Fluor 488 (1:500, Invitrogen, A21202); rabbit anti-DARPP32 (1:1000, Abcam, 40801), donkey anti-rabbit Alexa Fluor 594 (1:500, Invitrogen, A21207) or donkey anti-rabbit Alexa Fluor 647 (1:500, Invitrogen, A32795); goat anti-ChAT (1:100, Millipore, AB144P), donkey anti-goat Alexa Fluor 647 (1:500, Invitrogen, A21447) or bovine anti-goat Alexa Fluor 594 (1:500, Jackson ImmunoResearch, 805-585-180).

### Fluorescence in situ hybridization

In situ hybridization was performed using third-generation in situ hybridization chain reaction (HCR v3.0, Molecular Instruments). Zebra finch probe sequences were custom made by Molecular Instruments and designed using the NCBI database as a reference (VGLUT2, NM_001309508.1; tyrosine hydroxylase, XM_002198931.3; CHRNA4, XM_012570240.4). Adult male zebra finches were head-fixed on stereotaxic apparatus, and green RetroBeads (LumaFluor, G180) were injected into the sBG. Specifically, green RetroBeads were injected at three different ventral coordinates per hemisphere (3.1, 2.8, 2.6 mm; 75 nl for each site) in the sBG. One week after RetroBeads injection, consecutive sagittal sections were collected using the procedure described in 'Tissue collection'. Sections were post-fixed in 4% PFA for 20 min, followed by two 3-min washes in DEPC-PBS, a 45-min incubation in 5% SDS (Sigma, 71736) in DEPC-PBS and three 5-min washes in 2× sodium chloride sodium citrate 0.1% Tween 20 (2× SSCT, SSC, Invitrogen, AM9770; Tween, Sigma P9416). Then sections were pre-incubated in probe hybridization buffer (made by Molecular Instruments) for 30 min in a 37 °C incubator and transferred to probe hybridization buffer containing HCR probes (VGLUT2 and tyrosine hydroxylase, 1:200; CHRNA4, 1:50) overnight at 37 °C. On day 2, sections were washed in probe wash buffer (made by Molecular Instruments) for 30 min four times at 37 °C, followed by two 5-min washes in 2× SSCT at room temperature. Then sections were pre-incubated in a probe amplification buffer (made by Molecular Instruments) for 30 min at room temperature and transferred to a probe amplification buffer containing HCR fluorescent amplifiers at room temperature for 48 h. On the last day, sections were washed in 2× SSCT for two 5-min washes, incubated in Neurotrace (1:500) for 2 h, washed in 2× SSCT for two 5-min washes, coverslipped with Fluoromount-G (SouthernBiotech, 0100-01) and then imaged with a confocal microscope (Zeiss 710) for single-plane or *Z*-stack images, as needed. ImageJ with Fiji (v.1.51s, https://imagej.net/software/fiji/) was used for image analysis.

### Statistics and reproducibility

All analyses were two-tailed and we used $\alpha = 0.05$ as the threshold for significance. Statistical tests were performed using MATLAB (Mathworks), Prism (Graphpad), R and Python. The experiments were not randomized, and the investigators were not blinded to allocation during experiments and outcome assessment. For reproducibility, a summary of birds used in this study is in Extended Data Table 1.

### Reporting summary

Further information on research design is available in the Nature Portfolio Reporting Summary linked to this article.

## Data availability

Core datasets have been posted to the Duke University Library Research Data Repository (https://doi.org/10.7924/r4s186852). Source data are provided with this paper.

## Code availability

Custom codes are available at https://github.com/pearsonlab/autoencoded-vocal-analysis, https://github.com/SamuelBrudner/juvenile_syllable_analysis and https://github.com/denisecailab/ezTrack.


47. Hamaguchi, K. & Mooney, R. Recurrent interactions between the input and output of a songbird cortico-basal ganglia pathway are implicated in vocal sequence variability. *J. Neurosci.* **32**, 11671–11687 (2012).
48. Dan Foresee, F. & Hagan, M. T. Gauss-Newton approximation to Bayesian learning. In *Proc. International Conference on Neural Networks* 1930–1935 (IEEE, 1997).
49. Bates, D., Machler, M., Bolker, B. & Walker, S. C. Fitting linear mixed-effects models using lme4. *J. Stat. Softw.* **67**, 1–48 (2014).
50. Tibshirani, R. Regression shrinkage and selection via the lasso. *J. R. Stat. Soc. Series B Stat. Methodol.* **58**, 267–288 (1996).
51. Friedman, J., Hastie, T. & Tibshirani, R. Regularization paths for generalized linear models via coordinate descent. *J. Stat. Softw.* **33**, 1–22 (2010).
52. Lopes, G. et al. Bonsai: an event-based framework for processing and controlling data streams. *Front. Neuroinform.* **9**, 7 (2015).
53. Pennington, Z. T. et al. ezTrack: an open-source video analysis pipeline for the investigation of animal behavior. *Sci. Rep.* **9**, 19979 (2019).



**Acknowledgements** We thank A. Mercer for providing in situ hybridization and immunohistochemical data used to characterize the neurotransmitter phenotype of song premotor neurons. This research was supported by NIH grant no. 5R01 NS099288 to R.M., NIH grant no. RF1 NS118424 to R.M. and J.P., NIH grant no. F32 MH132152 to D.C.S. and NIH grant no. F31 NS132469 to M.M.


**Author contributions** J.Q., J.P. and R.M. planned the experiments. J.Q. conducted all experiments; D.C.S. helped conduct ACh fibre photometry experiments. J.Q., M.M. and D.C.S. analysed data with input from J.P. and R.M. J.Q. and R.M. wrote the manuscript. All authors edited the manuscript.

**Competing interests** The authors declare no competing interests.

**Additional information**


**Supplementary information** The online version contains supplementary material available at https://doi.org/10.1038/s41586-025-08694-9.



**Correspondence and requests for materials** should be addressed to John Pearson or Richard Mooney.



**Peer review information** *Nature* thanks the anonymous reviewers for their contribution to the peer review of this work. Peer reviewer reports are available.



**Reprints and permissions information** is available at http://www.nature.com/reprints.

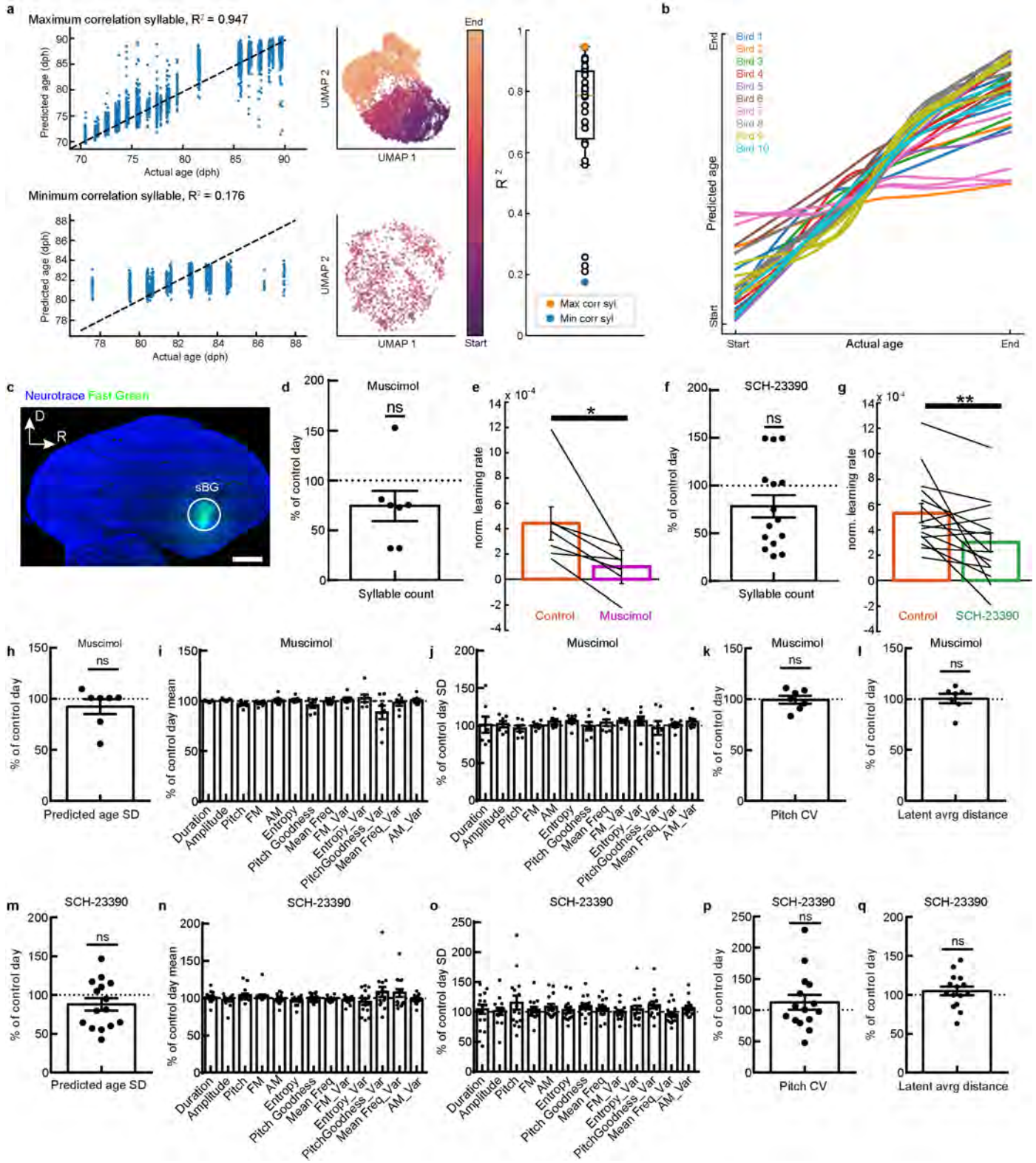


**Extended Data Fig. 1** | See next page for caption.

**Extended Data Fig. 1 | Effects of blocking neuronal activity and D1R-mediated signaling in the sBG on singing and song quality.** a) Predicted age scores (left) and latent distributions (middle) for the syllable with the highest (top row) and lowest (bottom row) correlation between predicted age and actual age. Heatmap indicates relative age of production. $R^2$ values for all syllables (34 syllables from 10 birds) are displayed in the rightmost column (box indicates median (0.786) and 1st (0.645), 3rd (0.866) quartiles, whiskers are quartiles +1.5 IQR (0.313, 0.947)). Predicted age scores for 30/34 syllables were highly correlated with actual age. b) Visualization of predicted learning trajectories for all syllables from (a). Learning trajectories, time-warped to the full imaging experiment of each DA and ACh bird used in the present study, 11.3 ± 4.2 days (mean, standard deviation). c) Representative histology of microdialysis experiments. Blue: neurotrace. Green: fluorescent dye (Fast Green) infused through the microdialysis probe to visualize drug spread. D: dorsal; R: rostral. Scale bar: 1 mm. d) Percentage of total syllable renditions produced on the muscimol day compared with the previous saline day ($n$ = 7 syllables from 5 birds; $t_6 = 1.678$, $p = 0.1443$, one sample two-tailed t-test). e) Group data showing that muscimol infusion into the sBG strongly reduced daily increase in predicted age scores, even when normalized to the total amount of singing (N = 7 syllables from 5 juveniles; $t_6 = 3.157$, $p = 0.0196$, two-tailed paired t-test). f) Percent total syllable renditions during the D1R blocking day compared with previous saline day (N = 15 syllables from 7 birds; $t_{14} = 1.868$, $p = 0.0828$, one sample two-tailed t-test). g) Group data showing that SCH-23390 strongly reduced the daily increase in predicted age scores, even when normalized to the total amount of singing (N = 15 syllables from 7 juveniles; $t_{14} = 3.036$, $p = 0.0089$, two-tailed paired t-test). h) Standard Deviation (SD) of Predicted Age following muscimol infusion relative to saline day (N = 7 syllables from 5 birds; $t_6 = 1.086$, $p = 0.3193$, one sample two-tailed t-test). i, j) Quantification of mean value (i) and standard deviation (j) of multiple acoustic features of individual syllables on the muscimol day compared with previous saline day (N = 7 syllables from 5 birds). For all features, $p > 0.05$, one sample two-tailed t-test with Bonferroni correction. k) Coefficient of Variation (CV) of Pitch following muscimol (N = 7 syllables from 5 birds; $t_6 = 0.1410$, $p = 0.8925$, one sample two-tailed t-test). l) Average distance to the mean syllable rendition in latent space (i.e., dispersion from the mean) after muscimol (N = 7 syllables from 5 birds; $t_6 = 0.08429$, $p = 0.9356$, one sample two-tailed t-test). m-q) As in (h-l), except for the D1-antagonist SCH-23390, N = 15 syllables from 7 birds. m) $t_{14} = 1.534$, $p = 0.1473$, one sample two-tailed t-test. n,o) $p > 0.05$ for all comparisons, one sample two-tailed t-test with Bonferroni correction. p) $t_{14} = 1.062$, $p = 0.3063$, one sample two-tailed t-test. q) $t_{14} = 0.8929$, $p = 0.3870$, one sample two-tailed t-test. FM: frequency modulation. AM: amplitude modulation. Var: variance. Freq: frequency. d-q: Boxes and error bars denote mean ± SEM. $^{*}p < 0.05$, $^{**}p < 0.01$, $^{***}p < 0.001$, ns: not significant. norm.: normalized.

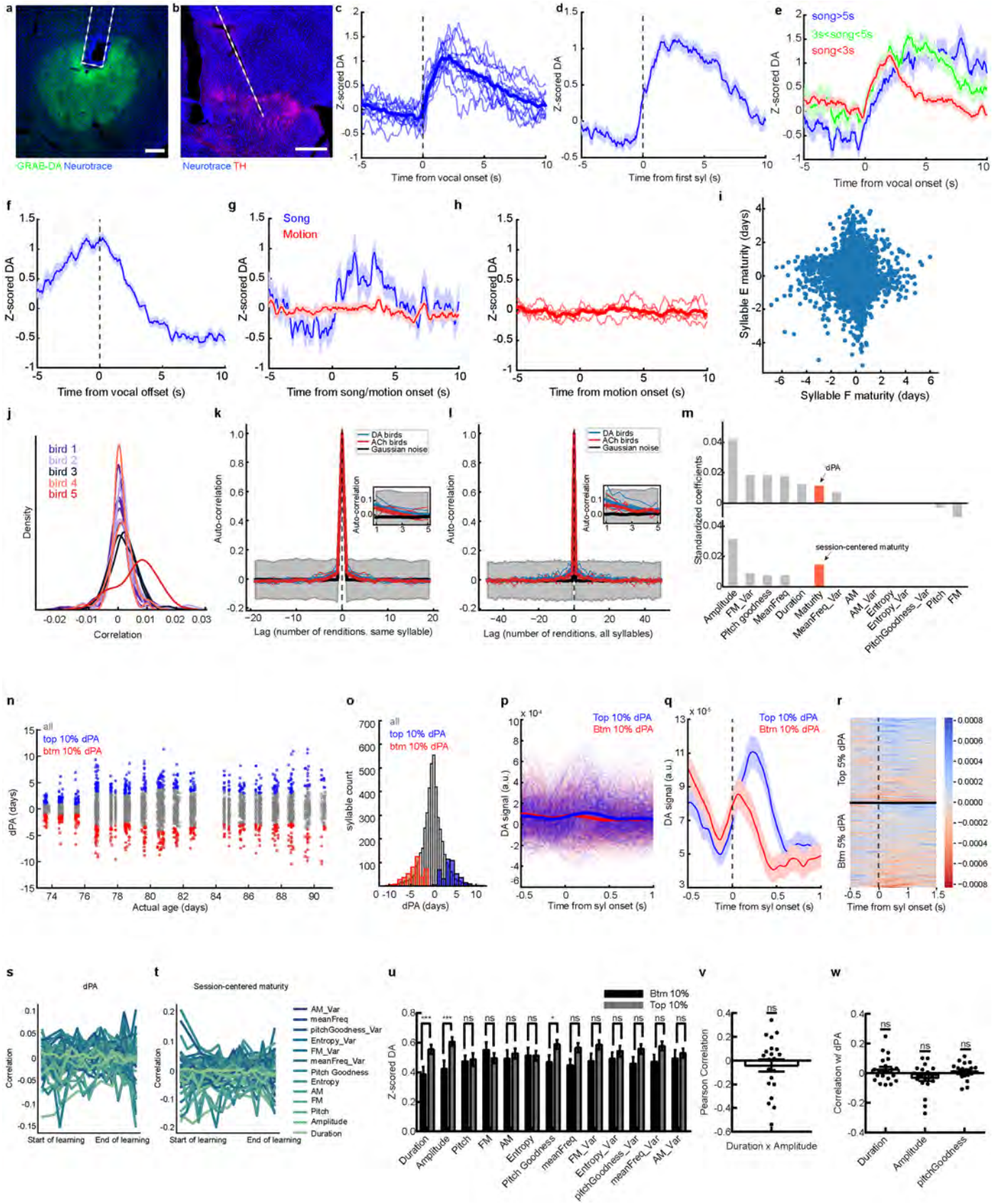


**Extended Data Fig. 2** | See next page for caption.

**Extended Data Fig. 2 | Singing-related DA transients in the sBG, predicted age analysis, and syllable acoustic features.** a) Representative histology of GRAB-DA2m photometric recordings. Green: GRAB-DA2m. Blue: neurotrace. White dashed line: placement of photometry ferrule. Scale bar: 200 µm. b) Representative histology of VTA stimulation in a GRAB-DA2m bird. Red: Tyrosine Hydroxylase. Blue: neurotrace. White dashed line: placement of the stimulating electrode. Scale bar: 500 µm. c) Mean z-scored DA traces for each of the 12 birds (light blue lines) and mean trace across the 12 birds (solid blue line), aligned to song onset. d) Representative GRAB-DA2m fluorescence in the sBG aligned to the first syllable in the motif (67 songs from the same bird as Fig. 2f). e) Representative GRAB-DA2m fluorescence in the sBG aligned to onset of song bouts of different duration. Red: song bouts <3 s (93 songs from one adult). Green: song bouts >3 s and <5 s (22 songs from the same bird). Blue: song bouts >5 s (20 songs from the same bird). f) Representative GRAB-DA2m fluorescence in the sBG aligned to song offset (66 songs from the same bird as Fig. 2f). g) Representative GRAB-DA2m fluorescence in the sBG aligned to 19 song and 155 motion onsets from the same recording session in one bird. h) The mean z-scored DA traces for each of the 5 birds (light red lines) and the mean trace across the 5 birds (solid red line), aligned to motion onset. i) Example of session-centered maturity of 5896 pairs of successive syllables (syllables E and F) from one bird. correlation = 0.0250. j) Distribution of correlation in session-centered maturity scores for 16 successive syllable pairs from 5 juveniles. 89% of syllable pairs (730/824 of recording sessions) did not show a significant correlation in session-centered maturity. Out of the significant pairs, the correlation was centered at zero (0.0049 ± 0.0008). k) Auto-correlation of maturity across renditions of the same syllable. Thin lines: single bird average. Thick lines: mean (across birds) ± SEM. Black lines are null distribution, with 95% CI (gray). l) Auto-correlation of maturity across renditions of all syllables. Lines as in (k) m) Coefficients of linear, LASSO-regularized model predicting mean DA (100-300 ms post syllable onset) from acoustic features and dPA (upper panel) and session-centered maturity (lower panel). Maturity retains its relationship with DA when accounting for acoustic features. n) Distribution of delta Predicted Age (dPA) scores for a single syllable from one juvenile across recording days (gray), with top 10% (blue) and bottom 10% (red) dPA scores from each recording day, as sampled for the group analysis in Fig. 2i–l. o) Histogram showing the distribution of dPA scores for all recording days from the syllable shown in I; all dPA scores (gray), with top 10% (blue) and bottom 10% (red) dPA scores from each recording day. p) Raw isosbestic-corrected DA transients for 443 renditions of the top (light blue lines) and 443 renditions of the bottom (light red lines) 10% of delta Predicted Age (dPA) renditions of the syllable show in Fig. 2i. Thick blue and red lines represent the mean of the two groups, which are also the blue and red lines in (q). q) Raw isosbestic-corrected DA transients for the top (blue, averaged from 443 renditions) and bottom (red, averaged from 443 renditions) 10% of delta Predicted Age (dPA) renditions of the syllable shown in Fig. 2i. r) A heatmap for raw isosbestic-corrected DA transients with an exponential moving average of prior DA transients subtracted, for top and bottom 5% renditions of the syllable shown in (q). s) Correlation between dPA and all acoustic features. Each line is the average correlation between dPA and an acoustic feature across syllables for a single bird, N = 5 juveniles. t) As in s) but between session-centered maturity and acoustic features. u) Mean z-scores of syllable-aligned DA transients (100-300 ms post onset) for top/bottom 10% of various acoustic features. N = 21 syllables from 5 birds; 2-way RM ANOVA significant interaction between Feature and Top/Bottom Decile; $F_{12,260} = 2.865$, $p = 0.0010$. Bonferroni corrected post hoc testing revealed that Duration ($t_{260} = 4.132$, $p = 0.0006$), Amplitude ($t_{260} = 4.454$, $p = 0.0002$), and Pitch Goodness ($t_{260} = 2.965$, $p = 0.0430$) significantly differed. v) Pearson correlation between Duration and Amplitude (N = 21 syllables from 5 birds; $t_{20} = 0.8353$, $p = 0.4134$, one sample two-tailed t-test). w) Pearson correlation between dPA and those features with significant DA relationships. At the group level, no feature was significantly correlated with dPA ($p > 0.05$, one-sample two-tailed t-test). d-g, q: Solid trace and shaded region indicate mean and SEM, respectively. u-w: Boxes and error bars denote mean ± SEM. $^{*}p < 0.05$, $^{**}p < 0.01$, $^{***}p < 0.001$, ns: not significant. FM: frequency modulation, AM: amplitude modulation. Var: variance. Freq: frequency.

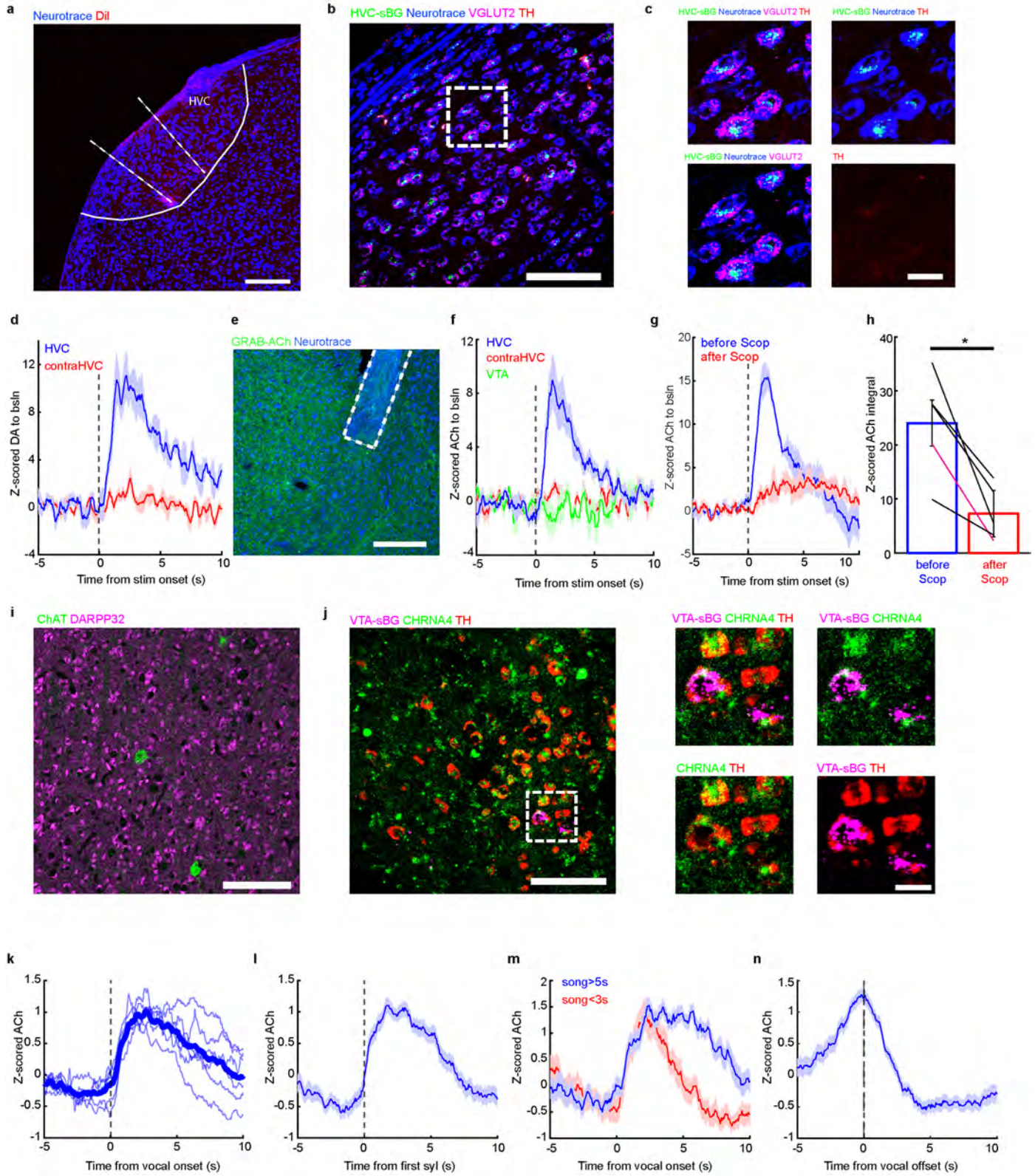


**Extended Data Fig. 3** | See next page for caption.

**Extended Data Fig. 3 | Song premotor control of dopaminergic and cholinergic signaling in the sBG.** a) Representative histology of HVC stimulation in a GRAB-DA2m bird. Red: DiI, used to coat the bipolar stimulating electrode to show electrode placement. Blue: neurotrace. White dashed line: placement of the bipolar stimulating electrode. Scale bar: 200 µm. b, c) Lower- (b) and higher-power (c) images showing that HVC neurons retrogradely labeled (green) by retrobead injection into the sBG express VGLUT2 mRNA (magenta), but not TH mRNA (red); all neurons are labeled with neurotrace (blue). Scale bar: 100 µm (left) and 20 µm (right). d) Example GRAB-DA2m transient evoked in the sBG by ipsilateral HVC stimulation (blue, 3 trials from one bird; similar results observed in 8 birds) and not by contralateral HVC stimulation (red, 5 trials from the same bird; similar results observed in 4 birds). e) Representative histology of GRAB-ACh3.0 photometric recordings. Green: GRAB-ACh3.0. Blue: neurotrace. White dashed line: placement of photometry ferrule. Scale bar: 200 µm. f) Example GRAB-ACh3.0 signals evoked in the sBG by ipsilateral HVC stimulation (blue, data from Fig. 3d) but not by contralateral HVC stimulation (red, 5 trials from the same bird, similar results observed in 7 birds) or ipsilateral VTA stimulation (green, 5 trials from the same bird, similar results observed in 5 birds). g) Example ACh evoked in the sBG by HVC stimulation before (blue, 5 trials) and after (red, 4 trials) systemic injection of scopolamine (Scop). h) Areal difference between ACh transients before/after scopolamine (0-2 s after stimulation, N = 5 adults; $t_4 = 4.474$, $p = 0.0110$, two-tailed paired t-test). Magenta line, example in (g). i) Representative histology showing expression of ChAT+ (green, a marker for cholinergic neurons) and DARPP32+ (magenta, a marker for spiny neurons) neurons in the sBG. Scale bar: 100 µm. j) Lower- (left) and higher-power (right) images showing that the VTA neurons that are retrogradely labeled (magenta) by injection of retrobeads in the sBG express both nAChRα4 mRNA (CHRNA4, green) and TH mRNA (red). Scale bar: 100 µm (left) and 20 µm (right). k) The mean z-scored ACh traces for each of the 6 birds (light blue lines) and the mean trace across the 6 birds (solid blue line). l) Representative GRAB-ACh3.0 fluorescence in the sBG aligned to the onset of the first syllable in the motif, 54 trials from one bird. m) Representative GRAB-ACh3.0 fluorescence in the sBG aligned to the onsets of song bouts of different song duration. Blue: song bouts <3 s (16 trials from one bird). Red: song bouts>5 s (22 trials from the same bird). n) Representative GRAB-ACh3.0 fluorescence in the sBG aligned to song offset, 70 trials from one bird). d, f, g, k-n: Solid trace and shaded region indicate mean and SEM, respectively. h: Boxes and error bars denote mean ± SEM. $^{*}p < 0.05$.

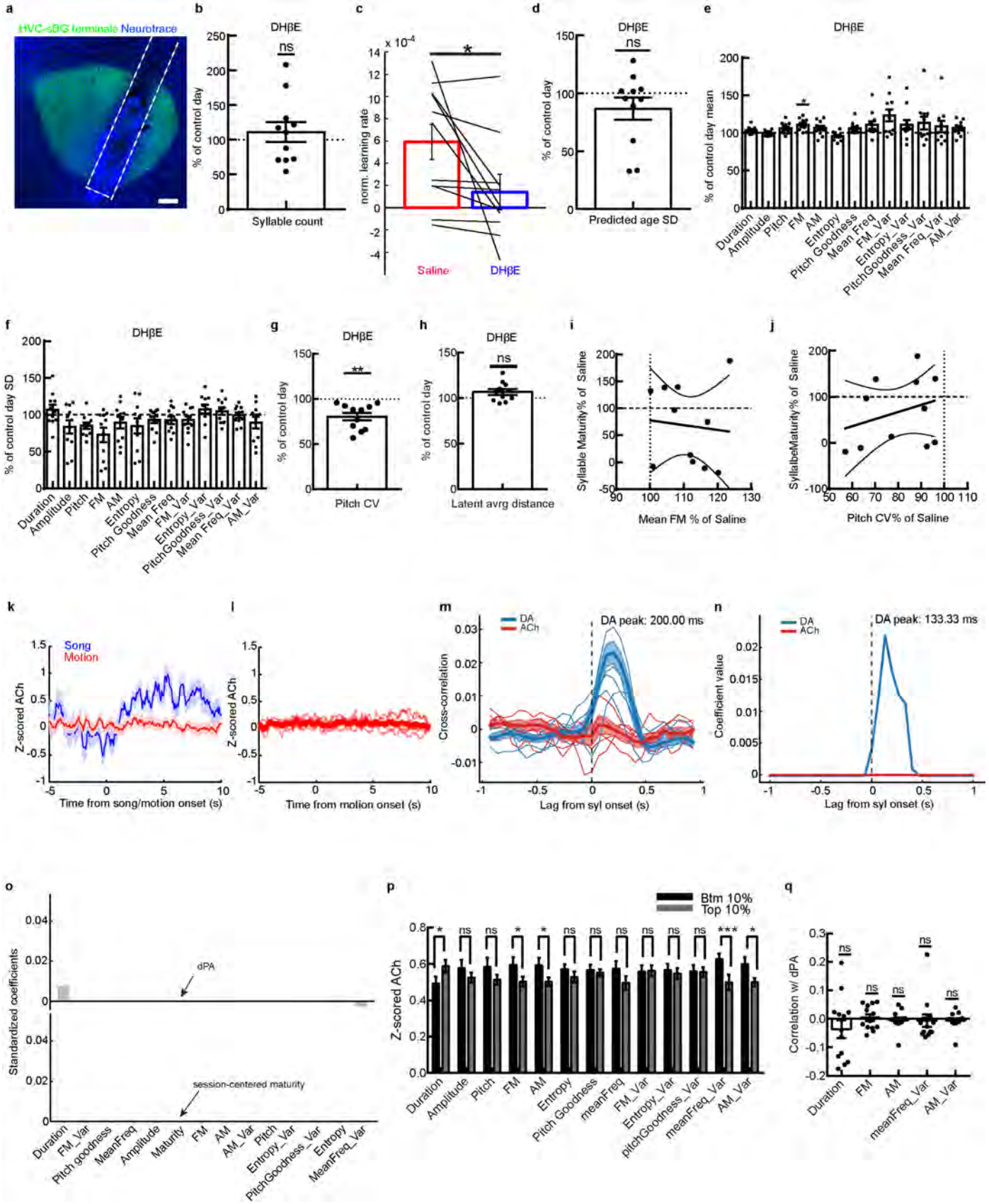


**Extended Data Fig. 4** | See next page for caption.

**Extended Data Fig. 4 | Effects of nicotinic acetylcholine blockers on singing and song features.** a) Representative DHβE microdialysis histology. Blue: neurotrace. Green: HVC terminals in the sBG labeled by injection of AAV2/9-CAG-GFP into HVC. White dashed line: microdialysis probe. Scale bar: 200 µm. b) Percentage of total syllable renditions produced on the DHβE treatment day compared with previous saline day (N = 11 syllables from 4 birds; $t_{10} = 0.7688$, $p = 0.4598$, one sample two-tailed t-test). c) DHβE reduced the daily increase in predicted age, even when normalized to the total amount of singing (N = 11 syllables from 4 juveniles, $t_{10} = 2.533$, $p = 0.0287$, two-tailed paired t-test). d) Standard Deviation (SD) of Predicted Age following DHβE infusion relative to saline day (N = 11 syllables from 4 juveniles, $t_{10} = 1.409$, $p = 0.1892$, one sample two-tailed t-test). e, f) Quantification of mean value (e) and standard deviation (f) of multiple acoustic features of individual syllables on the DHβE day compared with previous saline day (N = 11 syllables from 4 juveniles). For FM in e), $t_{10} = 4.771$, $p = 0.0104$. For all other features, $p > 0.05$. One sample two-tailed t-test with Bonferroni correction. g) Coefficient of Variation (CV) of pitch following DHβE (N = 11 syllables from 4 juveniles, $t_{10} = 4.551$, $p = 0.0011$, one sample two-tailed t-test). h) Average distance to the mean syllable rendition in latent space (i.e., dispersion from the mean) after DHβE (N = 11 syllables from 4 juveniles, $t_{10} = 2.107$, $p = 0.0613$, one sample two-tailed t-test). i) Change in mean FM and syllable maturity from DHβE relative to a preceding saline treatment. j) as in i) but for Pitch CV. Linear regressions revealed no significant relationship with syllable maturity for either mean FM ($F_{1,9} = 0.07644$, $p = 0.7884$, $R^2 = 0.008422$) or pitch CV ($F_{1,9} = 0.8336$, $p = 0.3850$, $R^2 = 0.08477$). k) Representative GRAB-ACh fluorescence in the sBG aligned to 14 song and 83 motion onsets from the same recording session in one bird. l) The mean z-scored ACh traces for each of the 5 birds (light red lines) and the mean trace across the 5 birds (solid red line), aligned to motion onsets. m) Cross-correlation between session-centered maturity and DA (blue) or ACh (red). Only DA was correlated with maturity. Mean cross-correlation (across birds) between DA and maturity peaked at 200 ms after syllable onset. Thin lines represent individual birds, dark lines represent the mean, and shaded region represents SEM. n) Lasso-regularized coefficients from sliding window analysis of session-centered maturity (see methods) for DA (blue) and ACh (red). All ACh coefficients are zero, while DA coefficients show a distinct peak at133ms after syllable onset, matching the cross-correlation analysis. o) Lasso-regularized coefficients from linear regression predicting mean z-scored syllable-aligned ACh transients (100-300 ms post onset) from acoustic features and dPA (o) or session-centered maturity (n). The majority of coefficients are zero, indicating no relationship between ACh and song maturity. p) Mean z-scores of syllable-aligned ACh transients (100–300 ms post onset) for top/bottom 10% of ACh for multiple acoustic features (N = 13 syllables from 5 birds; two-way RM ANOVA significant interaction between Feature and Top/Bottom Decile, $F_{12,156} = 3.837$, $p < 0.0001$. Bonferroni corrected post hoc testing revealed that Duration ($t_{156} = 3.182$, $p = 0.0230$), FM ($t_{156} = 3.087$, $p = 0.0306$), AM ($t_{156} = 3.019$, $p = 0.0379$), mean frequency variance ($t_{156} = 4.277$, $p = 0.0004$), and AM Variance ($t_{156} = 3.271$, $p = 0.0170$) significantly differed). q) Pearson correlation between dPA and those features with significant ACh relationships (N = 13 syllables from 5 birds). At the group level, no feature was significantly correlated with dPA ($p > 0.05$, one-sample two-tailed t-test). b-h, p, q: Boxes and error bars denote mean ± SEM. k, m: Solid trace and shaded region indicate mean and SEM, respectively. $^{*}p < 0.05$, $^{**}p < 0.01$, $^{***}p < 0.001$, ns: not significant. norm.: normalized. FM: frequency modulation, AM: amplitude modulation. Var: variance. Freq: frequency.

**Extended Data Table 1 | A summary of birds used in this study**

| Experiments | Condition | Figure | N of samples | N of birds | Histology confirmed? |
|---|---|---|---|---|---|
| Microdialysis | Muscimol | 1h-j, Ext. 1de, h-l | 7 syllables | 5 birds | Yes |
| | SCH-23390 | 1l-n, Ext. 1fg, m-q | 15 syllables | 7 birds | Yes except for 3 died before collecting brains |
| | DHBE | 4b-d, Ext. 4b-j | 11 syllables | 4 birds | Yes |
| Juvenile DA recording | DA maturity analysis | 2g-q, 4j, Ext. 2j-w, Ext. 4mn | 21 syllables | 5 birds | Yes |
| | DA motion analysis | Ext. 2gh | 5 birds | 5 birds | |
| Juvenile ACh recording | ACh maturity analysis | 4f-j, Ext. 4m-q | 13 syllables | 5 birds | Yes |
| | ACh motion analysis | Ext. 4kl | 5 birds | 5 birds | |
| Adult DA recording | DA, singing | 2ef, Ext. 2c-f | 12 birds | 12 birds | Yes except for 2 died before collecting brain |
| | DA, VTA stim | 2bc, | 8 birds | 8 birds | |
| | DA, HVC stim | 3b, Ext. 3d | 8 birds | 8 birds | |
| | DA, contralateral HVC stim | Ext. 3d | 4 birds | 4 birds | |
| | DA, white noise | 4mn | 7 syllables | 7 birds | |
| Optofluid cannula | HVC stim, before/after DHBE | 3km | 6 birds | 6 birds | Yes |
| | VTA stim, before/after DHBE | 3ln | 5 birds | 5 birds | |
| | singing, after saline/DHBE | 3s-v | 6 birds | 6 birds | |
| Adult ACh recording | ACh, singing | 3pq, Ext. 3k-n | 6 birds | 6 birds | Yes except for 1 died before collecting brain |
| | ACh, VTA stim | Ext. 3f | 5 birds | 5 birds | |
| | ACh, HVC stim | 3d, Ext. 3f | 7 birds | 7 birds | |
| | ACh, contralateral HVC stim | Ext. 3f | 7 birds | 7 birds | |
| | ACh, HVC stim before/after Scop | Ext. 3gh | 5 birds | 5 birds | |
| | ACh, white noise | 4op | 6 syllables | 6 birds | |
| Adult GFP control | GFP, singing | 2f | 4 birds | 4 birds | Yes |
| | GFP, VTA stim | 2c | 3 birds | 3 birds | |
| AAV1-Cre quantification | AAV1-Cre | 3f-i | 12 hemispheres (2 per bird) | 6 birds | Yes |
| *In situ* hybridization | HVC-sBG | Ext. 3bc | 2 hemispheres | 1 bird | Yes |
| | VTA-sBG | Ext. 3h | 2 hemispheres | 1 bird | Yes |

## Extended Data Table 2 | Blocking nAChRs in the sBG does not affect song duration

| effect | group | term | estimate | std.error | statistic | df | p.value |
|---|---|---|---|---|---|---|---|
| fixed | NA | (Intercept) | 5.296724428 | 0.823493666 | 6.432015988 | 5.027951575 | 0.001321699 |
| fixed | NA | TimeFactorAfter | 0.522173792 | 0.376775648 | 1.385901119 | 13.50142276 | 0.188242358 |
| fixed | NA | TreatmentFactorDHBE | 0.474566956 | 0.38571916 | 1.230343227 | 8.031513997 | 0.253384276 |
| fixed | NA | TimeFactorAfter:TreatmentFactorDHBE | -1.23876141 | 0.692100116 | -1.789858694 | 5.5752079 | 0.1274287 |
| random | bird | sd__(Intercept) | 1.94305213 | NA | NA | NA | NA |
| random | bird | cor__(Intercept).TimeFactorAfter | -1 | NA | NA | NA | NA |
| random | bird | cor__(Intercept).TreatmentFactorDHBE | 0.408614582 | NA | NA | NA | NA |
| random | bird | cor__(Intercept).TimeFactorAfter:TreatmentFactorDHBE | 0.040030024 | NA | NA | NA | NA |
| random | bird | sd__TimeFactorAfter | 0.416540308 | NA | NA | NA | NA |
| random | bird | cor__TimeFactorAfter.TreatmentFactorDHBE | -0.408614582 | NA | NA | NA | NA |
| random | bird | cor__TimeFactorAfter.TimeFactorAfter:TreatmentFactorDHBE | -0.040030024 | NA | NA | NA | NA |
| random | bird | sd__TreatmentFactorDHBE | 0.502657137 | NA | NA | NA | NA |
| random | bird | cor__TreatmentFactorDHBE.timeFactorafter:TreatmentFactorDHBE | -0.89561862 | NA | NA | NA | NA |
| random | bird | sd__TimeFactorAfter:TreatmentFactorDHBE | 1.215272746 | NA | NA | NA | NA |
| random | Residual | sd__Observation | 3.666646688 | NA | NA | NA | NA |

A linear mixed effects model was run to assess the effect of microdialysis infusions on song duration (ringers vs DHβE). Outcome variable: song duration. Fixed effects: treatment time (before or after treatment), treatment type (DHβE or control), and interaction. The interaction term reflects the effect of infusing DHβE on song duration. Random effect: bird.

nature portfolio

Corresponding author(s): Richard Mooney

Last updated by author(s): Jan 7, 2025

# Reporting Summary

Nature Portfolio wishes to improve the reproducibility of the work that we publish. This form provides structure for consistency and transparency in reporting. For further information on Nature Portfolio policies, see our Editorial Policies and the Editorial Policy Checklist.

## Statistics

For all statistical analyses, confirm that the following items are present in the figure legend, table legend, main text, or Methods section.

| n/a | Confirmed |
|---|---|
| ☐ | ☒ The exact sample size (*n*) for each experimental group/condition, given as a discrete number and unit of measurement |
| ☐ | ☒ A statement on whether measurements were taken from distinct samples or whether the same sample was measured repeatedly |
| ☐ | ☒ The statistical test(s) used AND whether they are one- or two-sided<br>*Only common tests should be described solely by name; describe more complex techniques in the Methods section.* |
| ☐ | ☒ A description of all covariates tested |
| ☐ | ☒ A description of any assumptions or corrections, such as tests of normality and adjustment for multiple comparisons |
| ☐ | ☒ A full description of the statistical parameters including central tendency (e.g. means) or other basic estimates (e.g. regression coefficient) AND variation (e.g. standard deviation) or associated estimates of uncertainty (e.g. confidence intervals) |
| ☐ | ☒ For null hypothesis testing, the test statistic (e.g. *F*, *t*, *r*) with confidence intervals, effect sizes, degrees of freedom and *P* value noted<br>*Give P values as exact values whenever suitable.* |
| ☒ | ☐ For Bayesian analysis, information on the choice of priors and Markov chain Monte Carlo settings |
| ☐ | ☒ For hierarchical and complex designs, identification of the appropriate level for tests and full reporting of outcomes |
| ☒ | ☐ Estimates of effect sizes (e.g. Cohen's *d*, Pearson's *r*), indicating how they were calculated |

*Our web collection on statistics for biologists contains articles on many of the points above.*

## Software and code

Policy information about availability of computer code

| | |
|---|---|
| Data collection | Sound Analysis Pro 2011 (http://soundanalysispro.com/) was used to collect song data in microdialysis experiments. A open-source software Bonsai was used to collect photometry data. White noise experiment was performed with a custom software program (EvTAF) (Tumer and Brainard 2007). ZEISS software was used to collect confocal images. |
| Data analysis | Autoencoded Vocal Analysis, the Python package used for the VAE analysis (AVA v0.3.1) is available online: https://github.com/pearsonlab/autoencoded-vocal-analysis. Artificial neural network (ANN) Matlab and Python package is available online: https://github.com/SamuelBrudner/juvenile_syllable_analysis. ezTrack used for tracking bird body position is available online: https://github.com/denisecailab/ezTrack. Sound Analysis Pro 2011 (http://soundanalysispro.com/) was used for song feature analysis. ImageJ with Fiji (version v1.51s, https://imagej.net/software/fiji/) was used for image analysis. For other data analysis and generation of figures,MATLAB (Mathworks, R2020b), Graph Prism (6.01 and 10.1.0), Python (3.10.12), and R (4.1.2) were used. |

For manuscripts utilizing custom algorithms or software that are central to the research but not yet described in published literature, software must be made available to editors and reviewers. We strongly encourage code deposition in a community repository (e.g. GitHub). See the Nature Portfolio guidelines for submitting code & software for further information.

## Data

Policy information about availability of data

All manuscripts must include a data availability statement. This statement should provide the following information, where applicable:

- Accession codes, unique identifiers, or web links for publicly available datasets
- A description of any restrictions on data availability
- For clinical datasets or third party data, please ensure that the statement adheres to our policy

Core datasets have been posted to the Duke University Library Research Data Repository (https://doi.org/10.7924/r4s186852).

## Research involving human participants, their data, or biological material

Policy information about studies with human participants or human data. See also policy information about sex, gender (identity/presentation), and sexual orientation and race, ethnicity and racism.

| | |
|---|---|
| Reporting on sex and gender | N/A |
| Reporting on race, ethnicity, or other socially relevant groupings | N/A |
| Population characteristics | N/A |
| Recruitment | N/A |
| Ethics oversight | N/A |

Note that full information on the approval of the study protocol must also be provided in the manuscript.

# Field-specific reporting

Please select the one below that is the best fit for your research. If you are not sure, read the appropriate sections before making your selection.

☒ Life sciences ☐ Behavioural & social sciences ☐ Ecological, evolutionary & environmental sciences

For a reference copy of the document with all sections, see nature.com/documents/nr-reporting-summary-flat.pdf

# Life sciences study design

All studies must disclose on these points even when the disclosure is negative.

| | |
|---|---|
| Sample size | No sample-size estimation was performed beforehand. Sample sizes were chosen in accordance with sample sizes used previously in birdsong learning studies:<br>Singh Alvarado J, Goffinet J, Michael V, et al. Neural dynamics underlying birdsong practice and performance. Nature. 2021;599(7886):635-639. doi:10.1038/s41586-021-04004-1<br>Kearney MG, Warren TL, Hisey E, Qi J, Mooney R. Discrete Evaluative and Premotor Circuits Enable Vocal Learning in Songbirds. Neuron. 2019;104(3):559-575.e6. doi:10.1016/j.neuron.2019.07.025<br>Hisey E, Kearney MG, Mooney R. A common neural circuit mechanism for internally guided and externally reinforced forms of motor learning. Nat Neurosci. 2018;21(4):589-597. doi:10.1038/s41593-018-0092-6 |
| Data exclusions | Experiments with unsuccessful surgery, injection, implantation, and expression were excluded from the data. For microdialysis experiments, birds singing song renditions less than 500 per day were excluded. |
| Replication | The results were based on behavior and recordings from multiple birds (as described in the text) and the reproducibility of the findings are shown in the group data. Birds were run in cohorts of 2-4 for microdialysis, and all other experiments were run in groups of 1-2 birds at a time due to the longitudinal nature of the study. We found similar results across cohorts. |
| Randomization | Animals were randomly allocated into experimental groups. |
| Blinding | No blinding was performed in this work. Blinding was impractical in most cases, especially in the longitudinal recordings. |

# Reporting for specific materials, systems and methods

We require information from authors about some types of materials, experimental systems and methods used in many studies. Here, indicate whether each material, system or method listed is relevant to your study. If you are not sure if a list item applies to your research, read the appropriate section before selecting a response.

## Materials & experimental systems

| n/a | Involved in the study |
|---|---|
| ☐ | ☒ Antibodies |
| ☒ | ☐ Eukaryotic cell lines |
| ☒ | ☐ Palaeontology and archaeology |
| ☐ | ☒ Animals and other organisms |
| ☒ | ☐ Clinical data |
| ☒ | ☐ Dual use research of concern |
| ☒ | ☐ Plants |

## Methods

| n/a | Involved in the study |
|---|---|
| ☒ | ☐ ChIP-seq |
| ☒ | ☐ Flow cytometry |
| ☒ | ☐ MRI-based neuroimaging |

# Antibodies

Antibodies used

Neurotrace 435/455 (Invitrogen, N21479), mouse anti-GFP (Invitrogen, A11120; clone 3E6), goat anti-mouse Alexa Fluor 488 (Invitrogen A11001), donkey anti-mouse Alexa Fluor 488 (Invitrogen, A21202), rabbit anti-DARPP32 (Abcam, 40801; clone EP720Y), donkey anti-rabbit Alexa Fluor 594 (Invitrogen, A21207), donkey anti-rabbit Alexa Fluor 647 (Invitrogen, A32795), goat anti-ChAT (Millipore, AB144P), donkey anti-goat Alexa Fluor 647 (Invitrogen, A21447), bovine anti-goat Alexa Fluor 594 (Jackson ImmunoResearch, 805-585-180), rabbit anti-TH (Millipore, AB152), goat anti-rabbit 488 (1:500, Invitrogen, A11034).

Validation

The primary antibodies have been widely used in rodents. GFP, TH, DARPP32 antibodies have been validated in zebra finches.
https://www.thermofisher.com/antibody/product/GFP-Antibody-clone-3E6-Monoclonal/A-11120
https://www.abcam.com/products/primary-antibodies/darpp32-antibody-ep720y-ab40801.html
https://www.sigmaaldrich.com/US/en/product/mm/ab144p
https://www.emdmillipore.com/US/en/product/Anti-Tyrosine-Hydroxylase-Antibody,MM_NF-AB152?ReferrerURL=https%3A%2F%2Fwww.google.com%2F
Singh Alvarado J, Goffinet J, Michael V, et al. Neural dynamics underlying birdsong practice and performance. Nature. 2021;599(7886):635-639. doi:10.1038/s41586-021-04004-1
Kearney MG, Warren TL, Hisey E, Qi J, Mooney R. Discrete Evaluative and Premotor Circuits Enable Vocal Learning in Songbirds. Neuron. 2019;104(3):559-575.e6. doi:10.1016/j.neuron.2019.07.025
Hisey E, Kearney MG, Mooney R. A common neural circuit mechanism for internally guided and externally reinforced forms of motor learning. Nat Neurosci. 2018;21(4):589-597. doi:10.1038/s41593-018-0092-6
In our study, the antibody for ChAT labeled large cell bodies in the striatum and basal forebrain, indicating it labels cholinergic neurons. DARPP32 densely labeled small cells in the striatum, as expected.

# Animals and other research organisms

Policy information about studies involving animals; ARRIVE guidelines recommended for reporting animal research, and Sex and Gender in Research

| | |
|---|---|
| Laboratory animals | Juvenile (31-95 dph) and adult (>120dph) male zebra finches (Taeniopygia guttata) |
| Wild animals | Not used |
| Reporting on sex | All animals used in this work were males, since only male songbirds learn to sing. |
| Field-collected samples | Not used |
| Ethics oversight | All experiments were performed in accordance with a protocol approved by Duke University Institutional Animal Care and Use Committee. |

Note that full information on the approval of the study protocol must also be provided in the manuscript.

# Plants

| | |
|---|---|
| Seed stocks | N/A |
| Novel plant genotypes | N/A |
| Authentication | N/A |